Osteoblast cell death triggers a pro-osteogenic inflammatory response regulated by reactive oxygen species and glucocorticoid signaling in zebrafish

Karina Geurtzen[1], Ankita Duseja[2], Franziska Knopf[1,*]

[1] CRTD - Center for Regenerative Therapies TU Dresden, Center for Healthy Aging TU Dresden, Germany

[2] Department of Oncology and Metabolism, Metabolic Bone Centre, Sorby Wing Northern General Hospital, Sheffield, UK

[*]Corresponding author:

franziska.knopf@tu-dresden.de, phone +49 (0) 351 458-82303

Key words (3-6)

Zebrafish, osteoblast, macrophage, ablation, glucocorticoid, reactive oxygen species, lineage tracing

Summary statement:

Laser-mediated osteoblast ablation induces recruitment of tissue-resident macrophages by a release of reactive oxygen species. The presence of macrophages is required for osteoblasts to repopulate the lesion site and can be modulated by glucocorticoids.

Abstract

In zebrafish, transgenic labeling approaches, robust regenerative responses and excellent *in vivo* imaging conditions enable precise characterization of immune cell behavior in response to injury. Here, we monitored osteoblast-immune cell interactions in bone, a tissue which is particularly difficult to *in vivo* image in tetrapod species. Ablation of individual osteoblasts leads to recruitment of neutrophils and macrophages in varying numbers, depending on the extent of the initial insult, and initiates generation of *cathepsinK*+ osteoclasts from macrophages. Induced osteoblast death triggers the production of pro-inflammatory cytokines and reactive oxygen species, which are needed for successful macrophage recruitment. Excess glucocorticoid signaling as it occurs during the stress response inhibits macrophage recruitment, maximum speed and changes the macrophages' phenotype. While osteoblast loss is compensated for within a day by contribution of committed osteoblasts, macrophages continue to populate the region. Their presence is required for osteoblasts to fill the lesion site. Our model enables visualization of homeostatic bone repair after microlesions at single cell resolution and demonstrates a pro-osteogenic function of tissue-resident macrophages in non-mammalian vertebrates.

Introduction

The skeleton and the immune system are close interaction partners, and crosstalk between both, which is controlled by a set of regulatory molecules (Takayanagi, 2007), influences bone formation and affects bone regeneration. Excessive and prolonged activation of inflammatory cells causes bone destructive diseases such as rheumatoid arthritis, while long term treatment with anti-inflammatory steroids causes osteoporosis (X. Feng & McDonald, 2011; Takayanagi, 2007). These diseases are associated with pain and fragile bone, and represent major health issues with strongly increasing incidence in the aging population (Odén et al., 2015).

After injury, recruitment of immune cells is the first step to ensure proper healing and to prevent the spread of inflammation (Duffield, 2003). Neutrophils dominate the early inflammatory response, becoming attracted to the respective sites immediately after the insult, in order to clear debris and recruit macrophages (Kolaczkowska & Kubes, 2013). This recruitment is initiated by various cytokine and chemokine stimuli released by neutrophils and apoptotic cells at the wound site (Duffield, 2003). Early arriving macrophages display an inflammatory phenotype and release cytokines to induce tissue degradation and cell apoptosis (Diez-Roux & Lang, 1997; Leibovich & Ross, 1975). Resolution of inflammation during later wound healing and tissue repair is promoted by anti-inflammatory macrophages (Novak & Koh, 2013). In the bone fracture environment, macrophage contribution is essential for deposition and mineralization of bone matrix (Andrew et al., 1994). In particular, macrophages initiate bone remodeling by direct interaction with osteoblasts and osteoclasts in damaged bone (Batoon et al., 2017; Jilka et al., 2007). Moreover, macrophages produce osteoactive molecules which promote osteogenic differentiation and mineralization (Pettit et al., 2008; Sinder et al., 2015). Conversely, interaction with osteoblasts can induce cells of the monocyte/macrophage lineage to differentiate towards osteoclasts (Quinn et al., 1998).

Zebrafish has emerged as a powerful animal model to study immunity and inflammation (C. Hall et al., 2009; Niethammer et al., 2009; Renshaw et al., 2006; Trede et al., 2004), bone metabolism, remodeling and skeletal disease (Banerji et al., 2016; Carvalho et al., 2017; Hayes et al., 2013; Kimmel et al., 2010; McNulty et al., 2012; Witten & Huysseune, 2009). Skeletal and immune cell biology are largely conserved among vertebrates, and zebrafish share the respective involved cell types, signaling pathways and molecules with mammals (Renshaw &

Trede, 2012; Witten & Huysseune, 2009). Compared to classic vertebrate models such as rodents (Brittijn et al., 2009) zebrafish research benefits from early and rapid bone development in the presence of optical transparency up to a late larval stage (Cubbage & Mabee, 1996). *In vivo* imaging of immune and skeletal tissue can be performed using a variety of transgenic tools labeling specific bone and immune cell types, enabling the visualization of cellular interactions in real time (Chen & Zon, 2009; Hammond & Moro, 2012).

Studies investigating the cellular reaction of zebrafish bone cells to injury have focused on the adult fin, in particular after amputation or cryoinjury (Ando et al., 2017; Chassot et al., 2016; Geurtzen et al., 2014; Knopf et al., 2011; Singh et al., 2012; Sousa et al., 2011), or on the zebrafish jaw (Ohgo et al., 2019; Paul et al., 2016; H. Zhang et al., 2015). During fin and scale regeneration, live imaging of injury-responsive osteoblasts identified their ability to migrate and dedifferentiate, but also revealed the importance of *de novo* osteoblast generation (Ando et al., 2017; Cox et al., 2018; Geurtzen et al., 2014). Larval zebrafish models have been employed to understand vertebrate bone development (Ahi et al., 2016; DeLaurier et al., 2019; Kimmel et al., 2010; Sharif et al., 2014; Tarasco et al., 2017) and to decipher pathomechanisms underlying congenital skeletal disease (Fiedler et al., 2018; Gistelinck et al., 2018; Tonelli et al., 2020). While *in vivo* imaging studies on immune cell recruitment after infection and injury of non-osseous tissues (axonal tissue, mesenchymal fin fold tissue) are widely used (Ellett et al., 2011; Tomoya Hasegawa et al., 2017; Isles et al., 2019; Li et al., 2012; Lieschke et al., 2001; Sanderson et al., 2015) sterile larval bone injury models are missing.

In this study, we present a novel laser-induced lesion paradigm in a developing skull bone in zebrafish, which provides a powerful tool to study the interaction between bone and immune cells *in vivo*. Using this model, we demonstrate the variable extent of immune cell recruitment in response to ablation of osteoblasts, illustrate the ablation-induced release of reactive oxygen species (ROS) and show that neutrophils, tissue-resident macrophages and *cathepsinK*+ osteoclast-like cells are attracted to dying osteoblasts, which are replenished by proliferation and migration of *osterix*+ osteoblasts. Macrophage recruitment is inhibited by the systemic application of antioxidants as well as glucocorticoid administration, which additionally changes macrophage phenotype. Ablation of macrophages by a nitroreductase-mediated approach leads to a reduction of osteoblasts at the lesion site. Our model can be used to elucidate the signals driving appropriate and disturbed macrophage and neutrophil

recruitment to injured bone tissue *in vivo*, which is relevant for a variety of inflammatory bone diseases and for bone cell turnover during tissue homeostasis.

Results

A 10 % ablation of opercular osteoblasts is quickly reversed and leaves opercular growth unaffected

UV laser mediated cell ablations, which lead to loss of fluorescent signal produced by transgenic fluorophore reporters (Morsch et al., 2017), are known to effectively kill target cells in zebrafish (Dehnisch Ellström et al., 2019; Mathias et al., 2006; Smutny et al., 2015). In order to create a confined lesion in bone and simulate osteoblast cell death, we performed osteoblast ablation in transgenic *osterix*:nGFP zebrafish larvae at 6 days post fertilization (dpf), in which osteoblasts of the forming gill cover (opercle) are labeled by GFP, by using specific UV laser settings at a spinning disk confocal microscope. We evaluated the cell damage performed by laser ablation by investigating the number of opercular osteoblasts with and without lesion at several time points. At 1 hour post lesion (hpl) we detected a prominent loss of GFP signal at the lesion site (**Fig. 1A**), which corresponded to a loss of approximately 10 % opercular osteoblasts (100 +/- 9,9 cells in uninjured vs. 87,4 +/- 10,2 cells in lesioned zebrafish, **Fig. 1B**). At 1 day post lesion (dpl), recovery of GFP fluorescence in the lesion site was observed, despite the fact that osteoblast numbers remained slightly (but not significantly) lower than in control fish (103,4 +/- 7,3 cells in uninjured vs. 93,5 +/- 10,1 cells in lesioned zebrafish). Complete recovery of osteoblast number was achieved at 2 dpl (110,9 +/- 10,6 cells in uninjured vs. 106,1 +/- 7,9 cells in lesioned zebrafish, **Fig. 1B**), illustrating the quick recovery of osteoblast numbers in laser ablated opercles.

Next, we characterized the effect of laser-assisted osteoblast lesions on opercle structure and growth. To evaluate opercle volume before and after lesion, we stained zebrafish larvae by alizarin red live staining, which labels calcified structures (Javidan & Schilling, 2004), and rendered the surface with the help of IMARIS software. Ablation of osteoblasts led to a distinct structural change of the calcified matrix in the form of two closely spaced rings in places where the laser had hit (arrow and insets in **Fig. 1C**). These marks could be observed for several days post lesion, and disappeared by 9 dpl (**Fig. 1C**). As these marks were quite

prominent, and because bone forming osteoblasts were ablated, we wondered whether a change in opercle volume would result from lesion. Notably, quantification of opercular volume across different stages showed that there were no significant differences between lesioned and respective control zebrafish larvae (uninjured vs lesioned, all *10^3 µm^3, 1 dpl: 47,7 +/- 11,0 vs. 47,0 +/- 5,6, 2 dpl: 52,08+/-9,9 vs. 53,4 +/- 11,1, 3 dpl: 49,4 +/- 12,5 vs. 58,9 +/- 4,1, 6dpl: 63,3 +/- 22,4 vs. 63,9 +/- 4,8, 9 dpl: 193,4 +/- 51,6 vs. 225,4 +/- 37,2, **Fig. 1D**). This indicates that osteoblast ablation does not grossly affect opercular growth rate, although a temporal and spatially restricted structural damage in mineralized matrix could be observed, and that osteoblast numbers recover very quickly after ablation of a significant portion of osteoblasts.

Fig.1

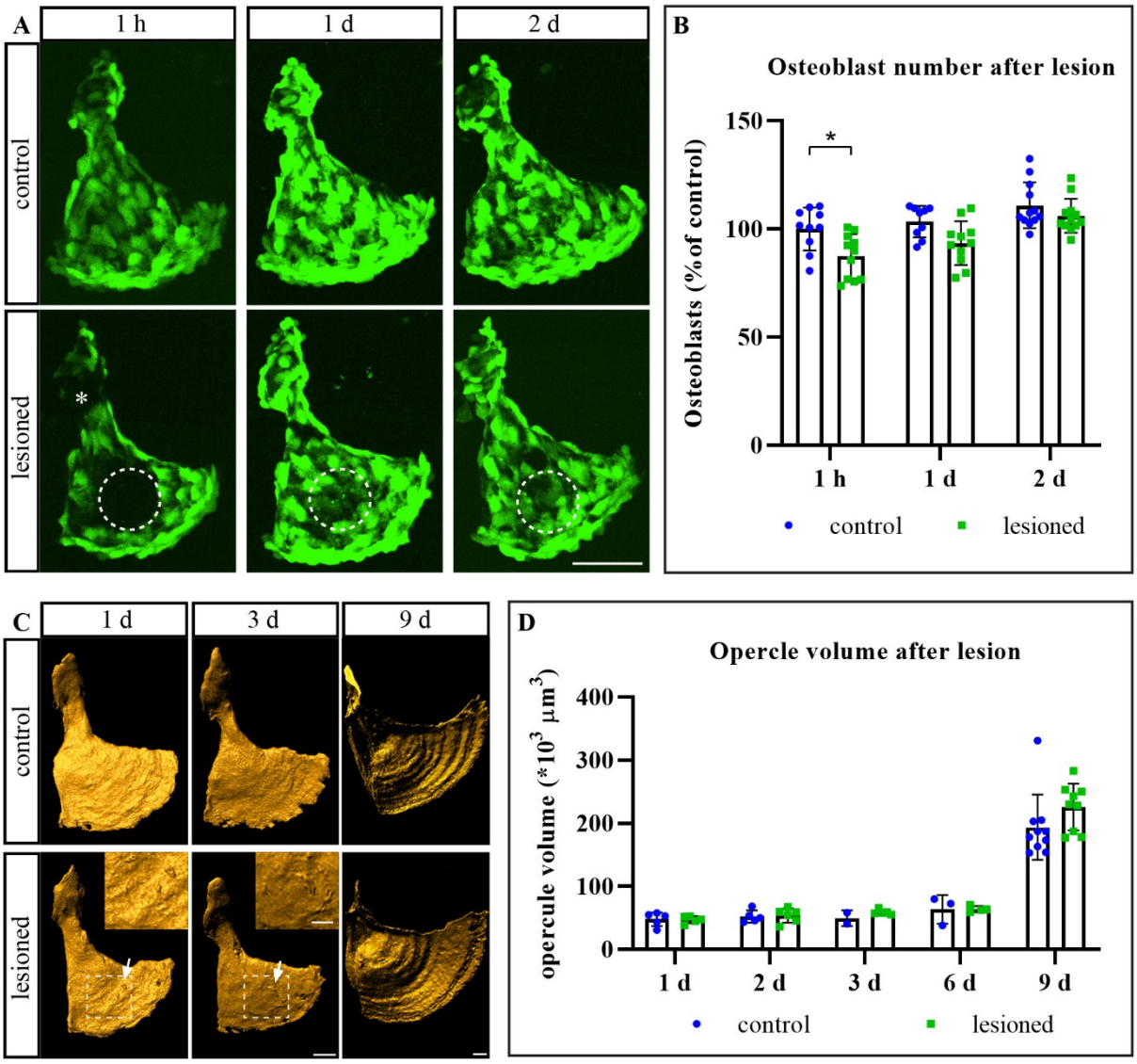

Fig. 1: Osteoblast recovery and unaffected opercular growth after laser ablation. A: Representative images of the opercle region in transgenic *osterix*:nGFP 6 dpf larval zebrafish. Loss of osteoblasts at 1 hpl and full recovery at 2 dpl can be observed. White dashed line = ablated area. Scale bar = 50 µm. **B**: Quantification of osteoblast numbers from experiment shown in A. About 10 % of the osteoblasts are ablated. Mean + s.d. Students-t-test: * p = 0.011. n = 9-12. **C**: Opercles of 6 dpf lesioned zebrafish stained with alizarin red. Boxed area with arrows and inset: Laser traces in the form of two spaced rings. Scale bar overview = 20 µm. Scale bar insets = 10 µm. **D**: Quantification of opercular volume from experiment shown in C. No significant differences can be observed. Mean + s.d. Sidaks' ANOVA. n = 3-10. h = hours, d = days.

Osteoblast numbers recover by proliferation and migration of committed osterix+ osteoblasts

Because quick recovery of osteoblast numbers was observed after lesion, we wondered how this recovery was accomplished. The most plausible explanation to us seemed to be the possibility that remaining osteoblasts proliferated in order to restore the necessary pool of osteoblasts. To test this, we performed live imaging of transgenic *osterix*:nGFP x *histone*:mCherry zebrafish larvae, in which nuclei of osteoblasts can be identified by co-localization of GFP and mCherry (Knopf et al., 2011), and by using *osterix*:nGFP transgenic animals. Although osteoblast proliferation occurred (**Movie 1**), it was a rare event (observed in 1 out of 15 larvae). At the same time, we observed slow relocation of pre-existing osteoblasts, as indicated by an increased number of osteoblasts reaching into the lesion site at 12 hpl (**Fig. 2A**). To confirm migration of pre-existing osteoblasts into the ablation site, we performed CreERT2-loxP mediated lineage tracing of *osterix*+ osteoblasts. *osterix*:CreERT2-p2a-mCherry x *hsp70*:R2nlsG double transgenic fish (Geurtzen et al., 2014; Hans et al., 2009; Knopf et al., 2011) were either treated with 4-hydroxytamoxifen (4-OHT) to induce CreERT2 activity and excision of a loxP-flanked DsRed Stop cassette in osteoblasts, or the vehicle control one day before the lesion (**Fig. 2B**). Three days post osteoblast ablation the resulting nuclear GFP+ osteoblasts representing recombined cells and their progeny were visualized with the help of a heat shock (**Fig. 2B, C**) (Geurtzen et al., 2014; Hans et al., 2009; Knopf et al., 2011). In 4-OHT treated larvae, GFP+ osteoblasts accumulated at the lesion site (**Fig. 2C**, white arrow), while no GFP+ cells were detectable in the vehicle control. These results indicate that committed *osterix*+ opercular osteoblasts move into the ablation site to replenish the lost osteoblasts, a process which is likely supported by proliferation of the very same cells. However, future assays will be needed to test the possibility of *de novo* osteoblast formation from alternative sources.

Fig.2

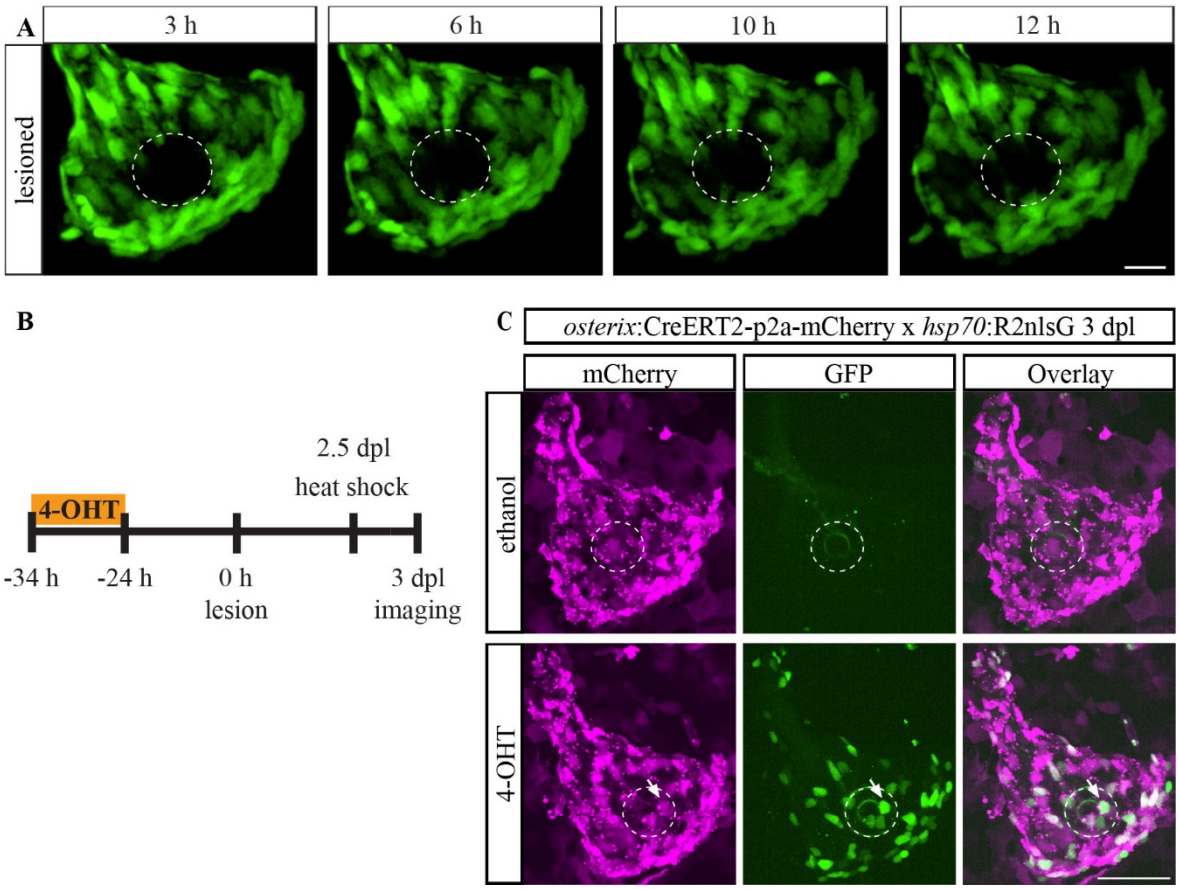

Fig. 2: Pre-existing *osterix*+ osteoblasts migrate into the lesion site after ablation. A: Images of opercular osteoblasts in 6 dpf transgenic *osterix*:nGFP larval zebrafish. Cellular extensions reach into the lesion site (area within white dashed line) within several hpl. Scale bar = 20 µm. n = 3. **B**: Scheme on CreERT2-loxP mediated lineage tracing approach of osteoblasts. Osteoblast ablation was performed at 6 dpf/12 h post 4-OHT/vehicle treatment. Two days later, a single heat shock was used to visualize nuclear GFP expression. **C**: Representative images of 4-OHT and vehicle treated *osterix*:CreERT2-p2a-mCherry x *hsp70*:R2nlsG larval zebrafish at 3 dpl (9 dpf). Pre-existing committed opercular osteoblasts are located at the lesion site (white arrow and dashed line). Scale bar = 50 µm. n = 5-7.

Osteoblast cell death leads to the release of immune cell attractants

Tissue damage and cell death lead to the release of a variety of chemokines and other cytokines, which have the potential to attract immune cells to the site of wounding (Duffield, 2003; Keightley et al., 2014). Furthermore, both processes enhance the expression of extracellular matrix (ECM) modifiers such as Matrix metalloproteinase 9 (Mmp9), a collagenase associated with inflammation which is found in wounded zebrafish (LeBert et al., 2015). We made use of transgenic *mmp9*:EGFP zebrafish (Ando et al., 2017) to test whether Mmp9 expression is induced in zebrafish bone tissue upon osteoblast ablation. While

occasional GFP fluorescence was observed in the lesioned area at 1 dpl, we detected robust induction of GFP at the lesion site at 2 dpl (uninjured vs. lesioned, 1 hpl: 109,6 +/- 1,5 units vs. 108,6 +/- 0,3 units, 1 dpl: 112,2 +/- 8,3 units vs. 126,1 +/- 18,9 units, 2 dpl: 109,9 +/- 0,2 units vs. 124,3 +/- 7,0 units, **Fig. 3A, B**). We set out to identify earlier signs of inflammatory cues after osteoblast ablation and turned to reactive oxygen species (ROS), which are known to be produced soon after acute wounding of other tissues such as the larval fin fold, where they are responsible for leukocyte attraction to the site of injury (Niethammer et al., 2009), or the tail (Romero et al., 2018). In order to test whether ROS were generated after laser-assisted osteoblast ablation, we pre-soaked *osterix*:nGFP larval zebrafish in CellROX orange dye, which starts to fluoresce upon ROS presence, performed lesions and concomitant *in vivo* imaging. Almost instantaneous activation of ROS-caused fluorescence was detected within a minute after ablation, and lasted throughout the imaging period of approximately 20 minutes. In contrast, control larvae which had not been lesioned but equally soaked in the CellROX orange dye, did not show any signs of fluorescence (**Fig. 3C, Movies 2 and 3**). These results indicate that sterile, laser-assisted ablation of a low number of bone forming cells triggers a similar response to injury as seen in other, more severe injury paradigms such as tissue resection. They also hint at a potential ability of the lesion paradigm to trigger recruitment of immune cells and osteoclasts (Callaway & Jiang, 2015), which, consequently, would allow the *in vivo* observation of leukocyte interactions with osteoblasts in bone tissue.

Fig.3

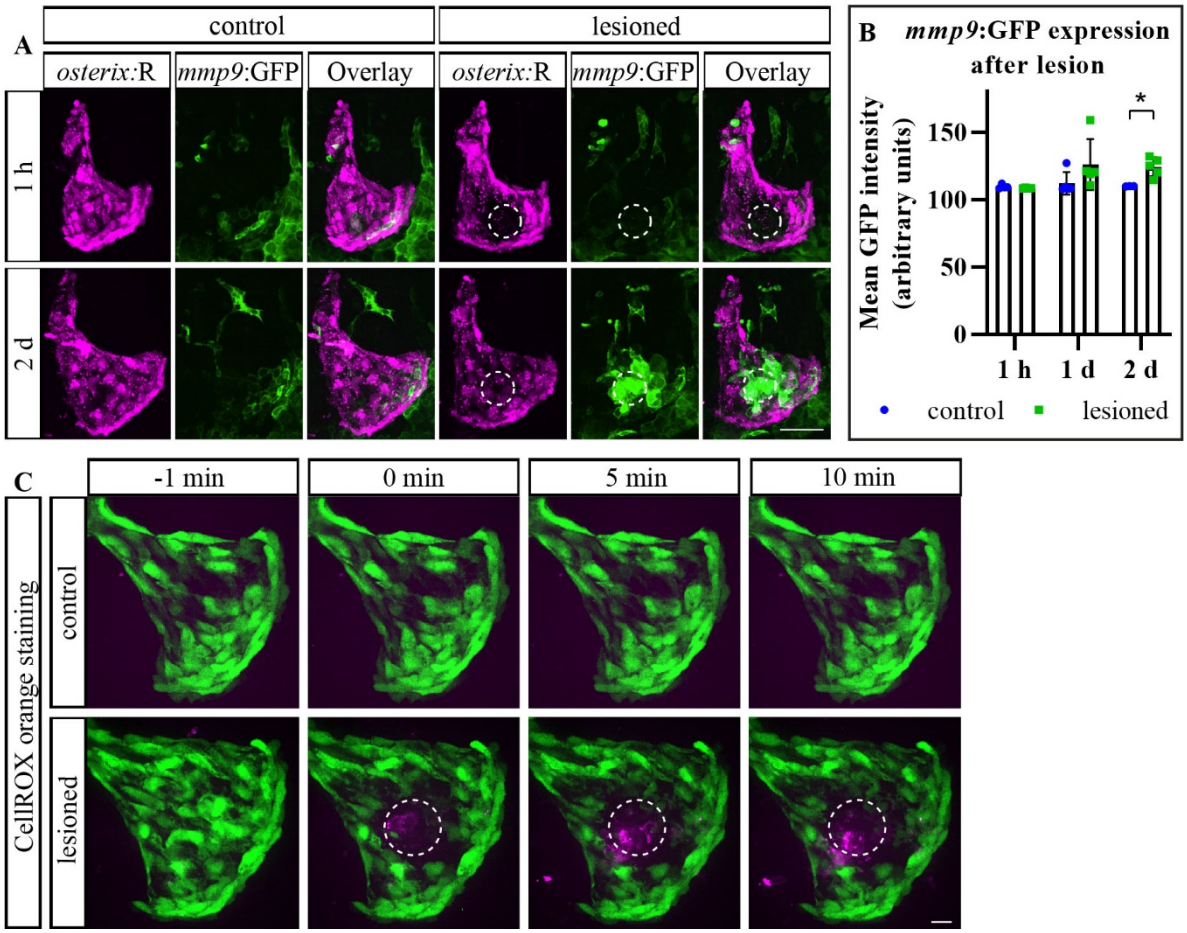

Fig. 3: Laser-assisted osteoblast ablation triggers Mmp9 production and ROS release. A: Transgenic *osterix*:RFP x *mmp9*:GFP lesioned zebrafish showing robust *mmp9* activity at 2 dpl. White dashed line = lesioned area. Scale bar = 50 µm. **B**: Quantification of experiment shown in A. At 2 dpl GFP is significantly increased. Mean + s.d. Welch's T-test: *p = 0.010. n = 3-5. **C**: CellRox orange staining of lesioned and unlesioned transgenic *osterix*:nGFP zebrafish larvae. ROS release is visible immediately after the laser lesion and increases over time in the ablation area (white dashed line). Scale bar = 10 µm. n = 6-7.

Neutrophils, inflammatory macrophages and osteoclast-like cells become recruited to the lesion site

Cell death and the release of corresponding signals serve as triggers for recruitment of immune cells (Duffield, 2003; Keightley et al., 2014). Increased levels of *mmp9*:GFP expression and ROS after osteoblast ablation prompted us to test whether neutrophil numbers change upon lesion. Live imaging of double transgenic *osterix*:RFP x *mpo*:GFP zebrafish larvae labeling osteoblasts and neutrophils at the same time revealed fast recruitment of neutrophils into the lesion area within minutes (**Fig. 4A** , **Movie 4**).

Similar to neutrophils, macrophages are attracted to the site of injury by cytokines and ROS (Mosser & Edwards, 2008). Moreover, early arriving neutrophils recruit macrophages to the injured or infected area after being the initial responders to the insult (Kolaczkowska & Kubes, 2013). We quantified the number of macrophages labeled by mCherry in double transgenic *osterix*:nGFP x *mpeg1*:mCherry zebrafish at different time points post lesion. While absolute macrophage numbers in the field of view did not change at 1 hpl, their number significantly increased until 1 dpl (uninjured vs. lesion, 1 hpl: 24,6 +/- 4,8 cells vs. 26,5 +/- 5,1 cells, 1 dpl: 25,3 +/- 5,2 cells vs. 37,3 +/- 8,3 cells, **Fig. 4B**), which suggests recruitment of macrophages to the lesion site after neutrophil arrival. Live-imaging using the above double transgenic zebrafish confirmed fast recruitment of macrophages that had resided in the field of view into the osteoblast-ablated area, as well of slightly delayed recruitment of macrophages from outside the field of view starting around 20 min (**Fig. 4C, Movie 5**). More than 50 % of macrophages passing the field of view during the imaging time were attracted into the lesion site during the first and second hour post lesion (1 hpl: 50,8 +/- 9,0 %, 2 hpl: 68,0 +/- 7,4 %, **Fig. 4D**). Live-imaging of *osterix*:nGFP x *mpeg1*:mCherry zebrafish combined with a transgenic marker for endothelial tissue, *kdrl*:CFP (Hess & Boehm, 2012), revealed that macrophages attracted to the lesion site arrive from within the tissues close to the lesion site and not from the blood stream, confirming their tissue-residency (**Fig. 4E, Movie 6**).

Fig.4

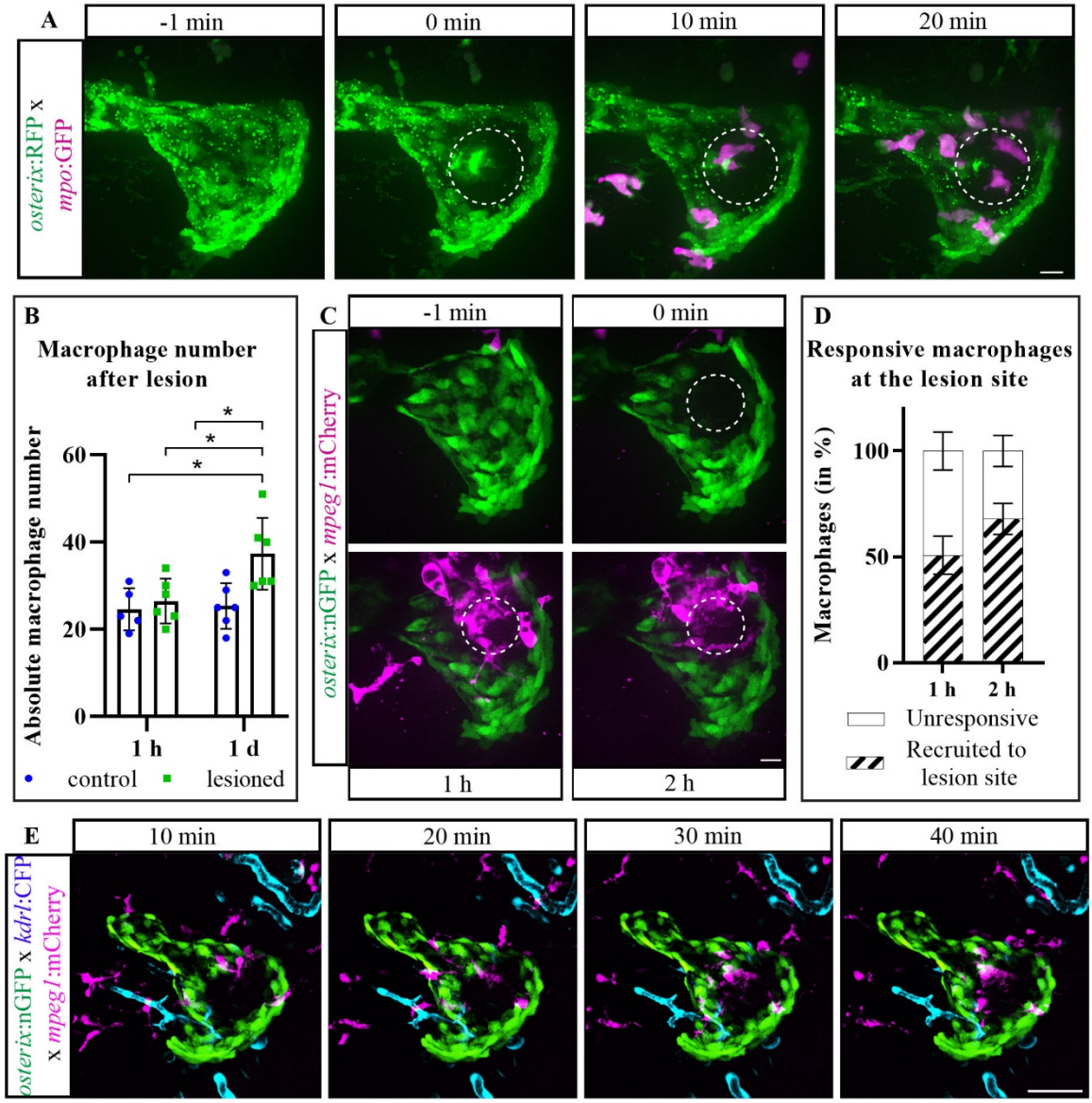

Fig. 4: Neutrophil and macrophage recruitment to the site of osteoblast ablation. A: Time series of the opercle region in transgenic *osterix*:RFP x *mpo*:GFP zebrafish (RFP depicted in green). *mpo*:GFP+ neutrophils, depicted in magenta, migrate into the ablation site (white dashed line) within several minutes post ablation. Scale bar = 10 µm. n = 7. **B**: Quantification of macrophage number in the opercle area. The number increases significantly after 1 day in lesioned opercles. Mean + s.d. Tukey's ANOVA: *p = 0.014 (1 d control vs. 1 d lesioned). n = 5-6. **C**: Time series of the opercle region of transgenic *osterix*:nGFP x *mpeg1*:mCherry zebrafish in which macrophages, depicted in magenta, migrate into the ablation site (white dashed line). Scale bar = 10 µm. **D**: Quantification of responsive macrophages migrating into the ablated area in the experiment shown in C. Mean + s.e.m. Sidak's ANOVA. n = 5. E: Time series of the opercle region of transgenic *osterix*:nGFP x *kdrl*:CFP x *mpeg1*:mCherry zebrafish showing that macrophages, depicted in magenta, are recruited from the surrounding tissue and not from blood vessels (ablation site indicated by white dashed line). Scale bar = 50 µm. n = 3.

Different macrophage subtypes and polarization stages can be observed in response to injury and inflammation (Stout et al., 2005). Early inflammatory responses are often associated with

the inflammatory type of macrophages (Duffield, 2003), also in zebrafish (Nguyen-Chi et al., 2015). Using triple transgenic *osterix*:nGFP x *mpeg1*:mCherry x *irg1*:EGFP zebrafish larvae in which activated macrophages (Sanderson et al., 2015) are labeled alongside osteoblasts, an increase in activated macrophages (mCherry/EGFP double+ migratory cells) was detected at 1 dpl (100,0 +/- 53,8 % in uninjured vs. 169,6 +/- 69,6 % in lesioned, white arrows in **Fig. 5A, B**). Similarly, the use of *tnf-α*:EGFP x *mpeg1*:mCherry transgenic zebrafish (Marjoram et al., 2015) demonstrated increased numbers of inflammatory macrophages at 1 and 2 dpl (uninjured vs lesioned, 1 hpl: 6,0 +/- 2,9 % vs. 5,6 +/- 1,7 %, 1 dpl: 9,4 +/- 5,5 % vs. 18,0 +/- 5,1 %, 2 dpl: 14,8 +/- 6,3 % vs. 24,2 +/- 9,4 %, white arrows in **Fig. 5C, D**). However, the majority of recruited macrophages at 1 and 2 dpl did not show the *tnf-α*+ inflammatory phenotype, which was only detected in about 20 % of all macrophages (1 dpl: 18,0 +/- 5,1 %, 2 dpl: 24,2 +/- 9,4 %, **Fig. 5D**).

Next, we combined the macrophage reporter with an osteoclast reporter line established in our laboratory, in which *cathepsinK*+ cells are labeled by nuclear mCherry (*ctsK*:nlsmCherry, **Fig. S1**). This approach enabled simultaneous observation of macrophages and osteoclast-like cells after lesion. Osteoclasts are known derivatives of monocyte/macrophage lineage cells, both in mammals (Quinn et al., 1998) and medaka (Phan, Liu, et al., 2020), another teleost fish species. Using triple transgenic *osterix*:nGFP x *mpeg1*:YFP x *ctsK*:nlsmCherry zebrafish we observed YFP/nlsmCherry double positive migratory cells several hours post lesion (white arrows in **Fig. 5E**). These cells were positive for *mpeg1* and *ctsK*, indicating that macrophages convert to *ctsK*+ osteoclasts after osteoblast ablation to some extent.

These results demonstrate that ablation of approximately ten cells in a confined region is sufficient to recruit leukocytes, and that the rapid recruitment of neutrophils is followed by attraction of inflammatory macrophages. This indicates the presence of a classic early wound response in the sterile laser-assisted bone lesion paradigm. Potential conversion of macrophages into osteoclasts suggests macrophages as a source for osteoclasts in larval zebrafish.

Fig.5

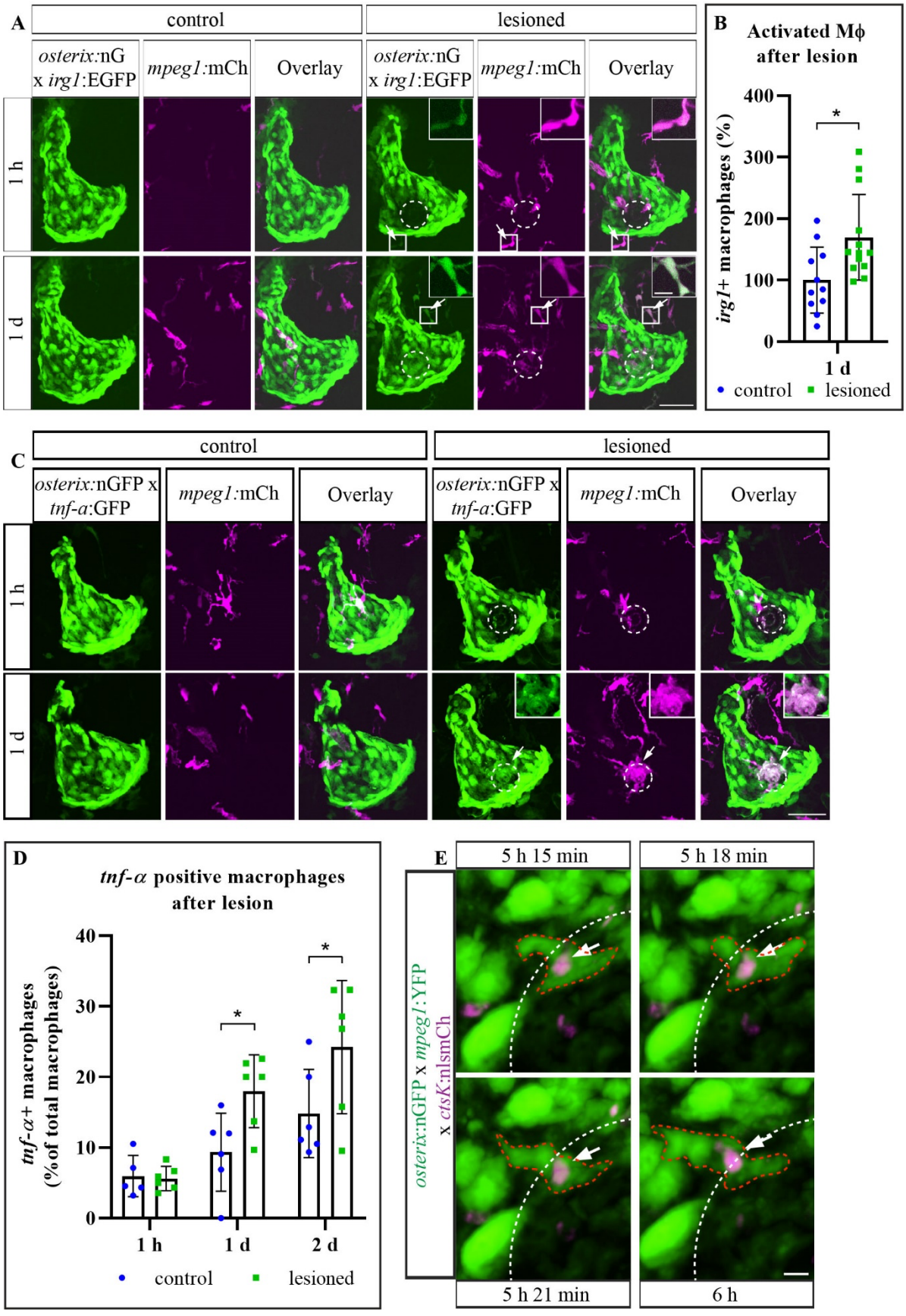

283

Fig. 5: Inflammatory macrophage and osteoclast presence after osteoblast ablation. A: Representative images of transgenic *osterix*:nGFP x *irg*:EGFP x *mpeg1*:mCherry uninjured and ablated zebrafish opercular regions. Activated macrophages can be detected in the lesioned opercle at 1 hpl and 1 dpl by co-expression of *irg1*:EGFP and *mpeg1*:mCherry (arrows and insets). Scale bar = 20 µm. **B**: Quantification of activated macrophage numbers after osteoblast ablation in experiment shown in A. Increased numbers of activated macrophages can be detected at 1 dpl. Mean + s.d. Welch's t-test: *p = 0.012. MΦ = macrophage. n = 11-13. **C**: Representative images of transgenic *osterix*:nGFP x *tnf-α*:GFP x *mpeg1*:mCherry zebrafish opercular regions. Inflammatory macrophages can be detected in the lesioned area (white dashed line) at 1 dpl by co-expression of *tnf-α*:GFP and *mpeg1*:mCherry (arrows and insets). Scale bar = 20 µm. **D**: Quantification of inflammatory macrophages after osteoblast ablation in experiment shown in C. Increased numbers of inflammatory macrophages can be detected at 1 and 2 dpl. Mean + s.d. Sidak's ANOVA: 1 dpl *p = 0.045, 2 dpl *p = 0.026. n = 5-6. **E**: Opercle region of transgenic *osterix*:nGFP x *mpeg1*:YFP x *ctsK*:nlsmCherry larvae at 5 to 6 hpl showing an *mpeg1*+, *ctsK*+ cell (white arrow and red dashed outline). White dashed line = border of the lesioned area. Scale bar = 5 µm. n = 4.

Antioxidant treatment suppresses macrophage attraction to the lesion site

Macrophages are attracted to their sites of action by oxidized proteins, lipids and cellular debris of apoptotic cells which are either exposed to or produce high levels of ROS (Tan et al., 2016). The presence of ROS has also been shown to be imperative for wound repair in fin fold and tail resected zebrafish larvae (LeBert et al., 2015; Romero et al., 2018). In order to assess the importance of ROS for immune cell recruitment and osteoblast recovery after laser-assisted cell ablation in bone, we treated larval zebrafish with DPI (diphenyleneiodonium chloride), a NADPH oxidase inhibitor which efficiently blocks ROS directly after fin fold amputation (**Fig. S2**) (Robertson et al., 2016), and assessed the recruitment of macrophages to the osteoblast ablation site. We observed limited recruitment of macrophages after DPI treatment **(Fig. 6, Movie 7)**, which indicates that production or release of ROS is essential for recruitment of macrophages to bone after osteoblast cell death.

Fig.6

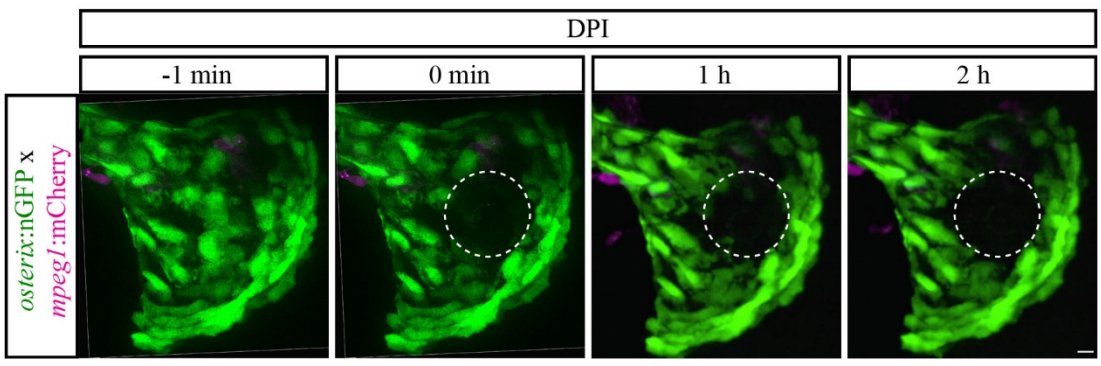

Fig. 6: Antioxidant treatment impairs macrophage recruitment to ablated osteoblasts. Time series of osteoblast-ablated, transgenic *osterix*:nGFP zebrafish, in which macrophage recruitment into the lesioned area (white dashed line) is blocked by a 5-hour pre-treatment with the antioxidant DPI. Scale bar = 10 µm. n = 6.

Immune-suppression by prednisolone alters macrophage recruitment to the lesion site

Macrophage activation and subtype specification need to be tightly controlled, otherwise an overexerted immune response might harm the tissue (Duffield, 2003). Persistent inflammation is also the cause for a variety of diseases that affect the skeletal system, such as rheumatoid arthritis which is routinely treated with glucocorticoids (den Uyl et al., 2011). These steroids inhibit the inflammatory response and particularly suppress macrophage recruitment in a variety of mammalian models (Cain & Cidlowski, 2017; Mosser & Edwards, 2008; Sharif et al., 2015). Making use of a previously established regime of larval zebrafish prednisolone treatment (Geurtzen et al., 2017), we tested whether mis-regulation of glucocorticoid receptor mediated signaling impacts (inflammatory) macrophage recruitment to the lesion site. After an 8-hour pre-treatment with prednisolone, which did not significantly alter the number of macrophages in the entire head of 6 dpf larvae (DMSO: 119,4 +/- 10,7 cells vs. pred: 110,4 +/- 16,92 **Fig. 7A**), and subsequent lesion, accumulation of macrophages at the lesion site was strongly reduced (**Fig. 7B, Movies 8 and 9**). A mere 10 % of the macrophages present in the opercle area were recruited into the lesion site during the first 2 hpl when prednisolone was administered, while more than 50 % of nearby macrophages were recruited to the lesion site in vehicle treated zebrafish (DMSO: 58,5 +/- 4,8 % vs. pred: 12,8 +/- 7,2 %, **Fig. 7C**).

We went on to test the impact of prednisolone on the appearance of *tnf-α*:EGFP+ inflammatory macrophages and determined the respective percentage of this inflammatory macrophage subtype in the opercle after treatment. Pre-treatment with the steroid significantly reduced inflammatory macrophage numbers as early as 1 hpl (DMSO vs. pred, 1 hpl: 19,1 +/- 8,8 % vs. 5,3 +/- 4,5 %, 1 dpl: 29,8 +/- 9,1 % vs. 13,7 +/- 12,4 %, **Fig. 7D, E**). These results show that glucocorticoids severely impair macrophage recruitment to microlesions in bone tissue, simultaneously suppressing their inflammatory activated phenotype.

Fig.7

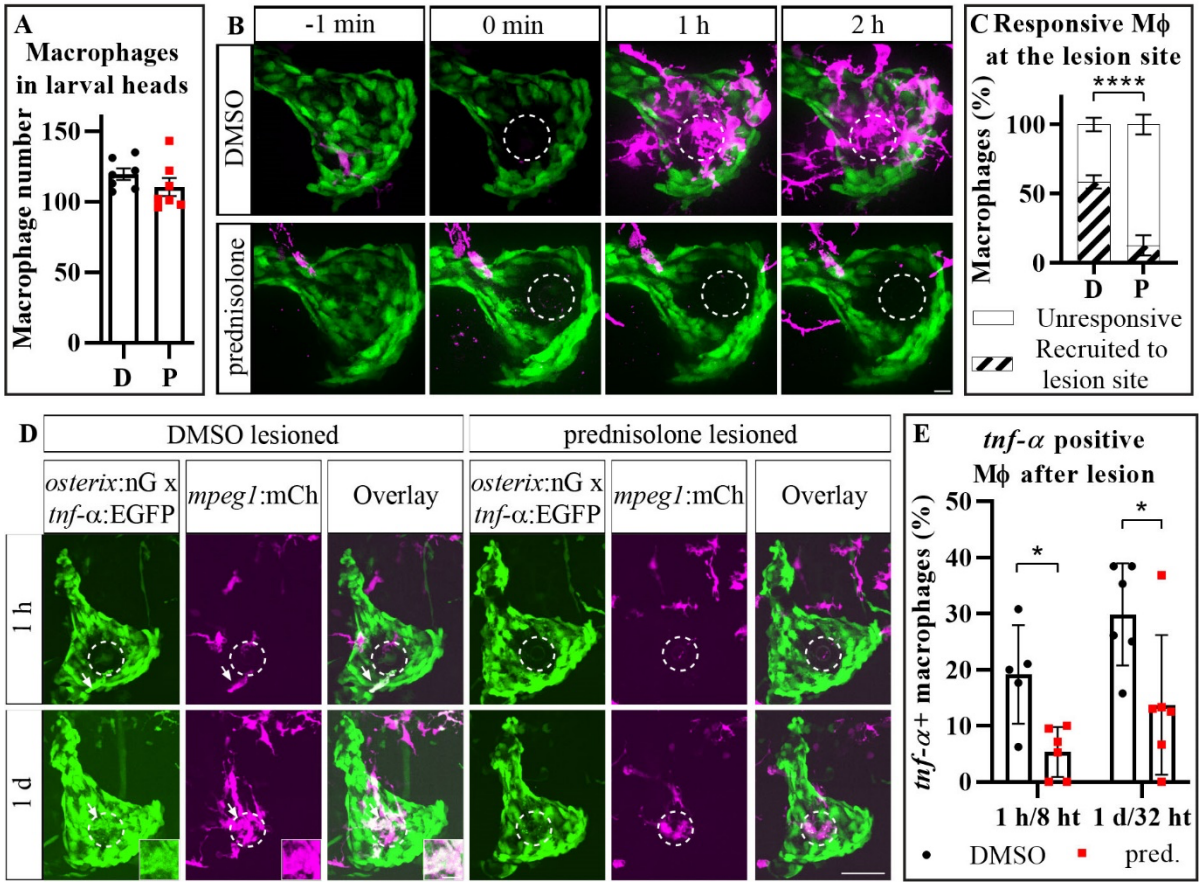

Fig. 7: Prednisolone treatment alters the recruitment of macrophages to the ablation site. A: The number of macrophages in the head of 6 dpf larval zebrafish after 8 ht (hours of treatment) with prednisolone is not altered compared to the control. Mean + s.e.m. Welch's t-test. n = 7. **B**: Time series of the opercular areas of transgenic *osterix*:nGFP x *mpeg1*:mCherry prednisolone and vehicle treated larvae. Prednisolone exposure strongly reduces the number of macrophages recruited into the lesioned area (white dashed line). Scale bar = 10 µm. **C**: Quantification of experiment shown in B. The number of responsive macrophages migrating into the lesioned area is significantly impaired by prednisolone treatment at 2 hpl. Mean + s.e.m. Sidak's ANOVA: ****p < 0.0001. n = 6-7. **D**: Representative images of transgenic *osterix*:nGFP x *tnf-α*:GFP x *mpeg1*:mCherry osteoblast-ablated zebrafish opercular regions after prednisolone treatment. While inflammatory macrophages can be detected in the lesioned area (white dashed line) at 1 dpl by co-expression of *tnf-α*:GFP and *mpeg1*:mCherry in the DMSO control fish (arrows and insets), their presence is impaired by prednisolone treatment. Scale bar = 20 µm. **E**: Quantification of experiment shown in D. Decreased numbers of inflammatory macrophages are detected in the opercle at 1 and 2 dpl in the prednisolone treated group. Mean + s.d. Sidak's ANOVA: 1 hpl *p = 0.044, 1 dpl *p =0.013. n = 5-6. MΦ = macrophage, D = DMSO, P = prednisolone, pred. = prednisolone.

Single-cell lesions allow the characterization of macrophage migratory features in response to osteoblast cell death and anti-inflammatory treatment

We asked ourselves whether smaller lesions causing cell death in fewer than 10 osteoblasts would reliably attract leukocytes to the site of lesion, a scenario potentially relevant to homeostatic tissue conditions, in which loading and cell senescence may lead to isolated cell death (Kennedy et al., 2012). In order to investigate macrophage recruitment and migration in more detail and to further study the effects of excess glucocorticoids on these features, we performed ablation of two to three osteoblasts in the center of the opercle (**Fig. 8A,** lesion outlined with white dashed line), and combined this with steroid drug administration. Recruitment of macrophages to the confined lesion site was apparent in both vehicle-treated and prednisolone-treated zebrafish (**Fig. 8B and Movies 10 and 11**); however, the relative contribution of nearby macrophages was strongly reduced compared to bigger lesions (big lesion 58,5 +/- 4,8 % vs. 18,1 +/- 8,7 % small lesion, both vehicle-treated). This indicates an injury-triggered dose-response-like mechanisms in leukocyte recruitment. In prednisolone-exposed larvae, a mild decrease of macrophage recruitment was evident (DMSO: 18,1 +/- 8,7 % vs. pred: 2,9+/- 2,9 % at 4 hpl, **Fig. 8C**), similar to what was observed after ablation of a higher number of osteoblasts. This strongly suggests that death of individual bone cells is detected by locally patrolling macrophages in otherwise unaffected tissue, and that anti-inflammatory treatment affects immune cell-osteoblast communication during tissue homeostasis.

The lower number of recruited macrophages in microlesions enabled us to track individual macrophages by ARIVIS 4D software and to analyze migration characteristics in undisturbed, vehicle treated zebrafish larvae versus individuals after glucocorticoid treatment (**Fig. 8D**). Migratory track analysis revealed an average macrophage speed of 25,1 +/- 4,7 nm/s in vehicle treated controls, which was mildly but not significantly reduced to 16,8 +/- 2,5 nm/s by prednisolone treatment (**Fig. 8E**). Similarly, prednisolone treatment exerted subtle (albeit insignificant) effects on macrophage straightness (DMSO: 0,13 +/- 0,02 units vs. pred: 0,09 +/- 0,01 units, **Fig. 8F**), a parameter describing directional migration of cells. Importantly, glucocorticoid administered zebrafish showed significantly reduced macrophage maximum speed (**Fig. 8G**), which was decreased to about half (216,4 +/- 32,29 nm/s in DMSO vs. 115,1 +/- 16,16 nm/s in prednisolone treated individuals). This illustrates the agility of macrophages on their way to the microlesion site, and demonstrates the stationary phenotype of macrophages upon excess glucocorticoid levels.

The lower number of macrophages attracted to the lesion site also allowed a detailed investigation of macrophage morphology and respective changes upon lesion in vehicle treated versus glucocorticoid treated zebrafish. Macrophages displayed an amoeboid morphology (**Fig. 8H**, macrophage outlined in blue) or changed into an amoeboid phenotype while migrating towards the lesion site in vehicle treated individuals (**Fig. 8H**, macrophage outlined in yellow). In contrast, macrophages had a ramified and elongated phenotype with several protrusions in prednisolone-exposed individuals (**Fig. 8H**, macrophage outlined in red). These results show that ablation of individual cells triggers a considerable immune response in zebrafish bone tissue, and that short-term glucocorticoid treatment affects macrophage morphology and migration.

Fig.8

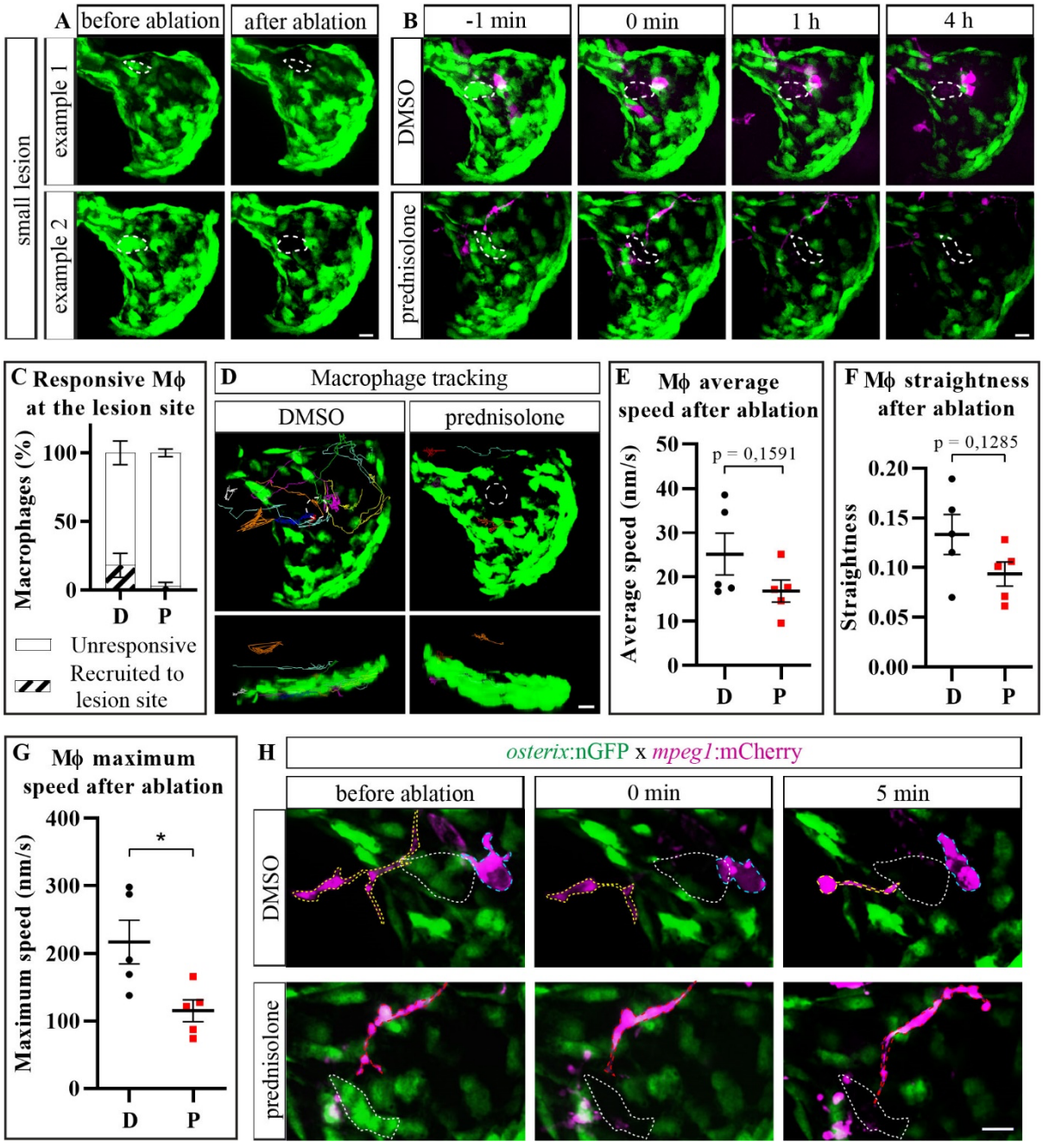

Fig. 8: Migratory features of macrophages in response to individual osteoblast ablation and prednisolone-treatment. A: Examples showing specific ablation of only a few isolated osteoblast cells in vehicle treated zebrafish (precise region of osteoblast ablation = white dashed line. Scale bar = 10 µm. **B**: Time series of the opercular region in transgenic *osterix*:nGFP x *mpeg1*:mCherry vehicle treated (same as example 2 in A) vs. prednisolone treated larvae with a small lesion. Prednisolone exposure reduces the number of macrophages (magenta) recruited into the lesioned area (white dashed line). Scale bar = 10 µm. **C**: Quantification of the experiment shown in B. The response of macrophages by migration towards and into the lesion area is slightly (though not significantly) impaired by prednisolone-treatment at 4 hpl. Mean + s.e.m. Sidak's ANOVA. n = 5. **D**: Representative images of individual macrophage tracking analysis in DMSO and prednisolone treated *osterix*:nGFP x *mpeg1*:mCherry larvae after small lesion. Arivis Vision 4D obtained tracks were overlaid with the first image after osteoblast ablation (upper panels = x-y view, lower panels = orthogonal view. Prednisolone treatment resulted in a lower number of

tracks and lacking migration into the lesion site. Scale bar = 10 µm. **E**: Quantification of the average macrophage speed using the tracking shown in D. Macrophages are slightly albeit not significantly slower after prednisolone treatment. Mean + s.e.m. Welch's t-test. n = 5. **F**: Quantification of macrophage straightness using the tracking shown in D. Straightness is slightly albeit not significantly reduced in prednisolone treated larvae. Mean + s.e.m. Welch's t-test. n = 5. **G**: Quantification of the maximum macrophage speed using the tracking shown in D. The maximum speed of prednisolone exposed macrophages is significantly lower. Mean + s.e.m. Welch's t-test: *p = 0.023. n = 5. **H**: Representative images of macrophages in the opercle region of *osterix*:nGFP x *mpeg1*:mCherry transgenic larvae treated with prednisolone or vehicle for 8 h. Time points shown: before, right after and 5 minutes post osteoblast ablation. White dashed line = region of ablated osteoblasts, blue dashed line = amoeboid macrophage, yellow dashed line = macrophage changing from ramified to amoeboid phenotype, red dashed line = ramified macrophage. Scale bar = 10 µm. MΦ = macrophage, D = DMSO, P = prednisolone.

As prednisolone treatment impaired macrophage recruitment to the ablation site and macrophages were recently suggested to promote osteoblast differentiation and bone mineralization in mammalian bone repair (Batoon et al., 2017), we investigated the effect of prednisolone administration on recovery of osteoblast numbers after lesion. We detected a significant reduction of osteoblasts in the opercle area after lesion of prednisolone treated zebrafish (DMSO 104,7 +/- 8,43 vs. pred. 92,3 +/- 6,62 cells, **Fig. 9A**), which indicated that macrophages may have a pro-osteogenic function in the repair of microlesions. To test this, we specifically ablated macrophages by a genetic nitroreductase (NTR)-mediated killing approach (Curado et al., 2008) in triple transgenic *osterix*:CreERT2-p2a-mCherry x *hsp70*:R2nlsG x *mpeg1*:YFP-NTR zebrafish (Petrie et al., 2014), and quantified the number of lineage-traced osteoblasts in the presence or absence of NTR (schematic **Fig. 9B**). Macrophage ablated samples showed a reduced number of lineage-traced, GFP+ osteoblasts at the lesion site (NTR- 2,73 +/- 0,90 vs. NTR+ 1,58 +/- 0,90 cells, **Fig. 9C, D**). In a separate experiment testing the impact of macrophage presence on general bone growth, osteoblast numbers were significantly reduced after a longer ablation period (NTR- vs. NTR+: 78,15 +/- 12,14 vs. 69,30 +/- 6,24 cells, **Fig. S3**).

In conclusion, manipulation of macrophage phenotype by pharmacologic glucocorticoid-treatment and their ablation by nitroreductase affect osteoblast recovery after microscopic bone lesion.

Fig.9

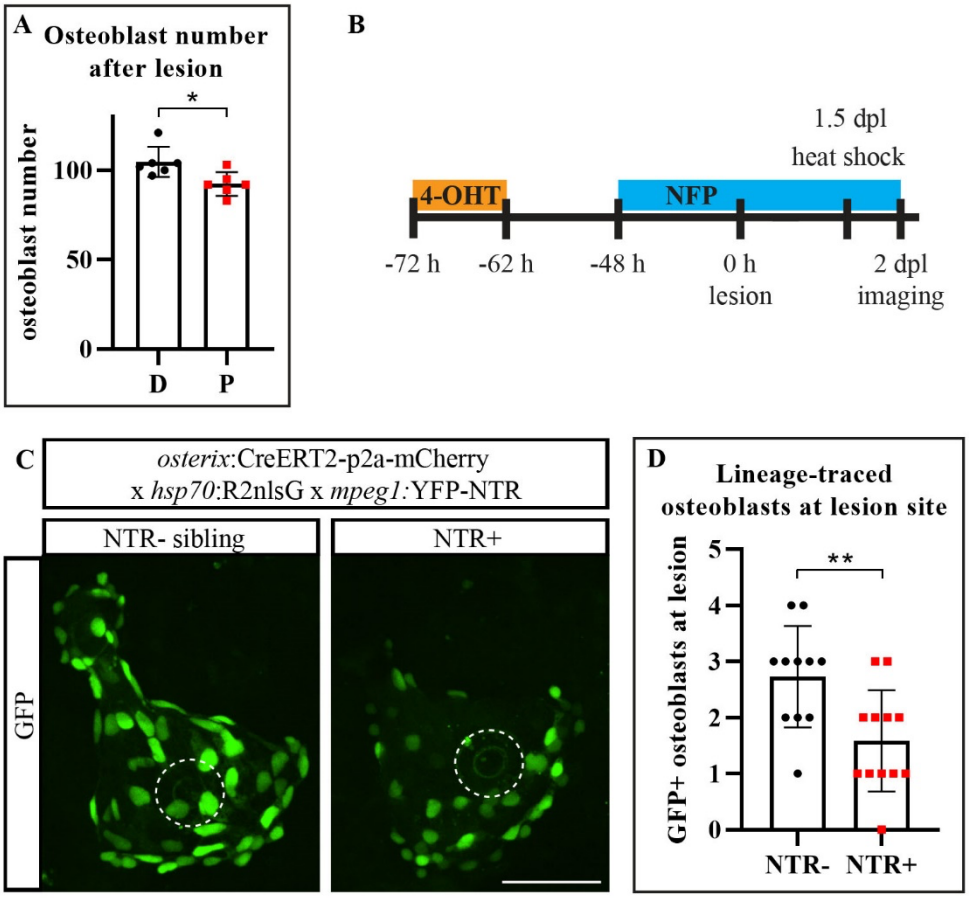

Fig. 9: Macrophage-ablation affects the recovery of osteoblasts after ablation. A: Quantification of the number of opercular osteoblasts in 7 dpf transgenic *osterix*:nGFP larval zebrafish after prednisolone treatment. Mean + s.d. Welch's t-test: *p = 0.019. n = 6. **B**: Scheme on NTR-mediated macrophage ablation combined with a CreERT2-loxP mediated lineage tracing approach of osteoblasts. Osteoblast ablation was performed at 6 dpf/72 h post 4-OHT/48 h post NFP treatment start. One day later, a single heat shock was used to visualize nuclear GFP expression. **C**: Representative images of 4-OHT and NFP-treated *osterix*:CreERT2-p2a-mCherry x *hsp70*:R2nlsG x *mpeg1*:YFP-NTR zebrafish and their NTR- siblings at 2 dpl. Macrophage ablation reduces the number of pre-existing committed opercular osteoblasts located at the lesion site (white dashed line). Scale bar = 50 µm. **D**: Quantification of experiment shown in C. Mean + s.d. Welch's t-test: **p = 0.006. n = 11-12. D = DMSO, P = prednisolone.

Discussion

Small teleost fish such as zebrafish and medaka have proven extremely useful to monitor bone tissue during regeneration *in vivo* (Chatani et al., 2011; Cox et al., 2018; De Simone et al., 2021; Knopf et al., 2011; Phan, Liu, et al., 2020), and to observe immune cell behavior in response to infection and non-sterile soft tissue injury (Barros-Becker et al., 2017; Gray et al., 2011; Gurevich et al., 2018; Li et al., 2012). Zebrafish lesion paradigms, mostly non-sterile,

have been developed for several tissues, also to study immune cell responses *in vivo* (Nguyen-Chi et al., 2015; Ohnmacht et al., 2016; Renshaw et al., 2006). Many studies make use of larval fin fold resection ('tail fin amputation') (Demy et al., 2017; LeBert et al., 2015; Nguyen-Chi et al., 2017; Niethammer et al., 2009). The fin fold has a simple architecture, consists of two epithelial layers innervated by sensory axons, encompasses actinotrichia and interspersed mesenchyme, and lacks bone entirely (O'Brien et al., 2012). Here, we have established an approach to specifically ablate bone forming osteoblasts in larval zebrafish *in vivo*, which we used to evaluate the immune cell response towards this spatially confined, tissue-specific lesion. Our model represents a valuable tool to study the immune cell response after microscopic bone lesion and provides the possibility to evaluate the recruitment and behavior of immune cells in contributing to a balanced bone cell turnover and repair.

Recovery after cell loss is essential to ensure tissue health and the same applies to osteoblasts whose function is essential for maintenance and repair of the skeleton (X. Feng & McDonald, 2011). Many cell populations have shown the potential to generate osteoblasts, summarized under the term skeletal stem cells in mammals (Serowoky et al., 2020). In zebrafish, osteoblasts self-renew by dedifferentiation and proliferation of mature osteoblasts (Geurtzen et al., 2014; Knopf et al., 2011; Sousa et al., 2011), but also become recruited from progenitor cell pools (Ando et al., 2017; Mcdonald et al., 2021). Notably, proliferation of osteoblasts could be observed in response to laser-assisted osteoblast ablation, albeit not frequently. In addition to proliferation, stretching of cellular processes of pre-existing *osterix*+ osteoblasts towards the lesion site at 1 dpl and lineage tracing of the very same cells confirm contribution of committed osteoblasts. A rapid contractile response mediated by actomyosin forces, such as seen in the resected fin fold within less than an hour (Mateus et al., 2012), is not seen. This can potentially be explained by the comparatively firm adhesion of osteoblasts to their matrix. In the future, cell cycle studies, e.g. by labeling cells with bromodeoxyuridine and anti-phosphohistone 3 antibodies, should be performed to quantify the contribution of proliferating cells to osteoblast recovery. A potential alternative source of osteoblasts located at the lesion site may be cells that generate osteoblasts *de novo* from a precursor-like state as seen in mammals, i.e. stromal cells or other cells reminiscent of mammalian skeletal stem cells, which needs to be tested in the future.

We did not detect developmental delays of bone formation after osteoblast lesion. This might be because of quick osteoblast recovery and due to the fact that opercular growth at the investigated developmental stages is comparatively slow; the volume of the opercular bone matrix increases only by about 10 % from 7 to 8 dpf (**Fig. 1C**). Furthermore, opercular growth mostly proceeds along the ventral-posterior bone edge with osteoblasts strongly concentrating in this region (Kimmel et al., 2010) which was also enriched for lineage-traced osteoblasts (**Fig. 2C**). The ventral-posterior edge of the opercle was not targeted in our lesion paradigm. It will be interesting to test whether osteoblast ablation in this region leads to a growth defect, and if so, how many osteoblasts would need to be ablated to evoke alterations.

One important process after wounding is the production and release of cytokines attracting immune cells, which is essential to initiate tissue repair (Duffield, 2003). Mmp9, one of the signals induced after tissue damage (LeBert et al., 2015; Matsubara et al., 1991), triggers leukocyte migration (Purwar et al., 2008). Similarly, high ROS amounts are released after wounding (Roy et al., 2006; Yoo et al., 2012) and stimulate recruitment of immune cells in zebrafish (Y. Feng et al., 2010; Niethammer et al., 2009). Sustained ROS levels are also observed after adult fin amputation, which includes the resection of bone (Gauron et al., 2013), and after resection of the larval notochord (Romero et al., 2018). Both *mmp9* activity and ROS production were induced by sterile laser-mediated osteoblast ablation as established in this work, which illustrates that ablation of less than a dozen cells causes a wound response comparable to the one seen after non-sterile, more severe wounding. However, *mmp9* activity was visualized with the help of a transgenic reporter, which requires several hours to mirror transcript activity of the *mmp9* gene, during which GFP protein is produced (Hazelrigg et al., 1998). For this reason, we cannot infer how fast *mmp9* message and protein are formed and whether Mmp9 release indeed plays a role in early leukocyte attraction. Conversely, rapid ROS release was visualized real time, and treatment with the antioxidant DPI reduced leukocyte attraction, indicating that ROS are involved. Classic work on zebrafish fin fold resection (Niethammer et al., 2009) and tumor-transformed skin cells (Y. Feng et al., 2010) demonstrated the importance of ROS-mediated immune cell attraction, which is likely to occur short-range (Jelcic et al., 2017). ROS blockage in our experiments may either cause reduced ROS levels at the ablation site or reduce ROS levels in macrophages, and therefore

lead to impaired recruitment. Notably, ROS accumulate in macrophages and other leukocytes playing an important role in leukocyte polarization (Robinson, 2008; Tan et al., 2016). Moreover, ROS production plays a crucial role in bone homeostasis promoting osteoclastogenesis and bone resorption (Bai et al., 2005; Lee et al., 2005), and oxidative stress is strongly associated with bone pathologies such as osteoporosis (Baek et al., 2010). However, to our knowledge ROS have not been visualized at cellular resolution *in vivo* in bone before, making this the first study to successfully label ROS release after osteoblast cell death in a living organism. It remains unclear, whether increase of ROS in or by individual osteoblasts is sufficient to attract immune cells. In the future, new tools such as KillerRed will enable tissue and cell type specific generation of ROS (Formella et al., 2018; Teh et al., 2010) in the growing opercle without ablating the cells. This will lead to the further characterization of the impact of ROS on bone cell turnover and tissue homeostasis.

In case of tissue damage a rapid immune cell influx is essential for efficient cell and tissue clearance and to ensure proper inflammation resolution and healing (Duffield, 2003). Both neutrophils and macrophages were recruited to the site of laser-assisted osteoblast ablation. Neutrophils were recruited first, and macrophages followed shortly after, which is in agreement with previous work (Keightley et al., 2014; Kolaczkowska & Kubes, 2013). The observed macrophages were tissue-resident, responded early, and might be responsible for later recruitment of monocyte-derived macrophages and other inflammatory leukocytes to the injury site (Davies et al., 2013). Moreover, the average speed of macrophages was comparable to previously reported zebrafish injury models (Barros-Becker et al., 2017; Ellett et al., 2011; Li et al., 2012). Furthermore, acquisition of *ctsK* expression in some macrophages, indicating osteoclast differentiation, was observed. A similar process was suggested to take place in medaka fish, in which RANKL (Receptor activator of NF-κB ligand) was ubiquitously overexpressed (Phan, Liu, et al., 2020; Phan, Tan, et al., 2020). Some caution is warranted, as *ctsK* also labels mesenchymal cells in some tissues (Debnath et al., 2018; Lu et al., 2020) and we observed immobile *ctsk*:nlsmCherry+ nuclei at a distance from the opercle, in locations unlikely to contain osteoclasts (data not shown). It is noteworthy that conversion of macrophages to osteoclasts depends on inflammatory signals such as Tnf-α (Phan, Liu, et al., 2020). We detected increased expression of *tnf-α* in some macrophages recruited to the lesion site, and these cells are good candidates for differentiation into osteoclasts. Further

550 investigation of additional osteoclast-specific and inflammatory marker gene expression, such
551 as of tartrate-resistant acid phosphatase, will reveal the importance of macrophage
552 recruitment and inflammatory phenotype for osteoclastogenesis at the lesion site.
553 Macrophage contribution to wound healing is dependent on the subtype characteristics.
554 Generally, the early wound-response is characterized by inflammatory macrophage action
555 marked by inflammatory cytokine release and phagocytosis of dead cells and debris (Duffield,
556 2003; Lieschke et al., 2001). Later phases are dominated by regenerative macrophage
557 responses leading to inflammation resolution and tissue remodeling (Duffield, 2003; Novak &
558 Koh, 2013). In zebrafish, transgenic reporter lines enable investigation of macrophage
559 phenotypes throughout inflammation and its resolution (Ellett et al., 2011; Gray et al., 2011;
560 Walton et al., 2015). Available tools showed that, similarly to the mammalian situation, two
561 waves of macrophages (inflammatory and regenerative) emerge in soft zebrafish tissues after
562 resection (Nguyen-Chi et al., 2017).
563 In this work, we evaluated the amount of activated and inflammatory macrophages at
564 relatively early time points post cell ablation. Interestingly, increased *irg1*:GFP+ macrophages
565 were already detected at 1 hpl indicating that these activated macrophages respond fast.
566 While Irg1 is not a direct read-out for the inflammatory macrophage phenotype, but instead
567 labels activated macrophages (Sanderson et al., 2015), it is often expressed in a pro-
568 inflammatory environment (Jamal Uddin et al., 2016) by pro-inflammatory macrophages
569 (Sanderson et al., 2015). We therefore conclude that activated macrophages populate the
570 lesion site early on and that they become polarized towards the inflammatory phenotype.
571 Notably, only about 25 % of macrophages in the opercle area and at the lesion site were
572 identified as inflammatory macrophages at 1 dpl, on the basis of *tnf-α*:GFP expression. This is
573 in agreement with work on fin fold resected zebrafish, in which approximately 30 % of
574 inflammatory macrophages were reported at 24 hours post amputation, although more
575 inflammatory macrophages could be detected earlier (Nguyen-Chi et al., 2017). In our model,
576 laser-assisted osteoblast ablation will allow to study the kinetics of the inflammatory
577 response to cell death in bone tissue, in particular with respect to normal and dysregulated
578 resolution of inflammation.
579
580 Tight regulation of the immune response is essential for wound healing and tissue repair, and
581 overexerted actions can be harmful in many inflammatory disorders (Duffield, 2003). In the

582 bone microenvironment, a variety of inflammatory conditions and therapy-associated
583 diseases such as rheumatoid arthritis and glucocorticoid-induced osteoporosis affect bone
584 health (den Uyl et al., 2011; X. Feng & McDonald, 2011; Takayanagi, 2007). In order to develop
585 novel therapies for such diseases and to counteract adverse effects of immunosuppressive
586 treatment, it is crucial to precisely understand how immune cells are affected in these
587 conditions. Zebrafish fin fold regeneration models combined with high dose glucocorticoid
588 treatment (Chatzopoulou et al., 2016; C. J. Hall et al., 2014; Sharif et al., 2015) showed that
589 glucocorticoids suppress the attraction of macrophages and neutrophils and impair tissue
590 regeneration. Here, by using a previously established larval prednisolone administration
591 regime (Geurtzen et al., 2017) on laser-ablated zebrafish larvae, we investigated the effect of
592 glucocorticoids on immune cells *in vivo* in the context of bone cell turnover and microscopic
593 bone repair. Particularly inflammatory macrophages were affected by prednisolone exposure,
594 as reported previously (Cain & Cidlowski, 2017; Russo-Marie, 1992; Xie et al., 2019).
595 Morphology, which can be used as a readout for activation and polarization status of
596 macrophages (McWhorter et al., 2013), was evidently altered after prednisolone exposure.
597 Inflammatory, activated macrophages display an amoeboid morphology with few dendrites
598 while anti-inflammatory macrophages are more elongated and display more dendrites, also
599 in zebrafish (Nguyen-Chi et al., 2015). Prednisolone exposure impaired the activated,
600 amoeboid morphology of macrophages in our model. Consistently, *tnf-α*:GFP+ macrophage
601 numbers dropped in prednisolone treated zebrafish, similar to effects after fin fold resection
602 and concomitant treatment (Nguyen-Chi et al., 2015).
603 Contrasting data have been obtained concerning the effect of glucocorticoids on immune cell
604 migration, also varying depending on the glucocorticoid used (Chatzopoulou et al., 2016;
605 Sharif et al., 2015; Xie et al., 2019). While beclomethasone leaves macrophage migration
606 unaffected in fin fold resected zebrafish (Chatzopoulou et al., 2016; Xie et al., 2019), high dose
607 dexamethasone treatment reduces macrophage recruitment in the same model (Sharif et al.,
608 2015). Here, we used prednisolone, a third synthetic glucocorticoid, to test for its
609 immunosuppressive effects after individual osteoblast ablation. Treatment led to a reduced
610 macrophage migratory ability in terms of maximum speed and number of recruited
611 macrophages. This is in agreement with previous results on adult bony fin ray-amputated
612 zebrafish, in which prednisolone treatment led to impaired macrophage accumulation in fin
613 regenerates (Geurtzen et al., 2017).

High dose glucocorticoids are known to strongly affect osteoblasts by inducing osteoblast apoptosis while impairing osteoblast proliferation and maturation (den Uyl et al., 2011; Weinstein, 2012). To date, it is unclear whether these anti-osteogenic effects are exclusively mediated directly or whether alteration of macrophage number and phenotype contribute to these effects. During mammalian bone repair, macrophages promote osteoblast differentiation and bone mineralization (Pettit et al., 2008), in particular after fracture (Batoon et al., 2017). In our lesion model, ablation of macrophages led to reduced osteoblast numbers at the lesion site, reflecting either impaired proliferation or migration of *osterix*+ osteoblasts. Decreased osteoblast numbers in the developing opercle after macrophage ablation point to a similar compromising effect, which was also observed in fractured mouse bones after tissue-resident macrophage ablation (Alexander et al., 2011; Batoon et al., 2017). This illustrates the capacity of tissue-resident macrophages to support bone formation in mammalian and non-mammalian vertebrates. In the future, it will be interesting to test osteoblast and macrophage- specific knockout tools in zebrafish, e.g. to delete the glucocorticoid receptor *nr3c1*, or to target prednisolone to phagocytic macrophages specifically to decipher the indirect negative impact of glucocorticoid exposure on osteoblasts via immune cells. Moreover, it will be interesting to compare anti-migratory effects of different synthetic glucocorticoids on macrophages and neutrophils across different wounding assays and tissues, specifically when taking bone tissue into account.

In vivo and intravital imaging approaches in rodent species have progressed a lot in recent years. Tissues such as the lung (Yang et al., 2018), kidney (Peti-Peterdi et al., 2016) but also bone (J. Kim & Bixel, 2020) have been investigated. A variety of studies examined the interaction of bone producing cells with immune cells by using *in vivo* microscopy (Tetsuo Hasegawa et al., 2019; Ishii et al., 2010; Kikuta et al., 2013). Ishii and colleagues used two-photon confocal laser microscopy to observe osteoclast precursor migration to bone tissues in homeostatic conditions (Ishii et al., 2009). Similar approaches, some of which making use of bone explants, facilitated imaging of osteoblast – osteoclast interactions, osteoprogenitors during cranial bone defect repair and the mechanism of osteocyte embedding into bone ECM (Dallas & Moore, 2020; Furuya et al., 2018; Huang et al., 2015; Shiflett et al., 2019). Albeit these advancements, limiting factors in terms of imaging depth persist for *in vivo* imaging of

rodent bone tissue. Furthermore, the ability to resolve cellular dynamics in terms of cell shape changes, migratory behavior and cell to cell contacts remains challenging. This is also true for long-term imaging of rodent bone tissue *in vivo*, which, in contrast, can be performed up to several days in zebrafish larvae (Kaufmann et al., 2012).

Laser-assisted approaches have a long tradition in zebrafish since they provide good tissue penetration (Morsch et al., 2017) and fine spatio-temporal control of manipulation (Johnson et al., 2011). This makes the system useful for a wide array of experiments triggering regeneration, such as by laser-induced axotomy (Hu et al., 2018), induction of thrombosis (Jagadeeswaran et al., 2006), cell ablation in the brain (Sieger et al., 2012), spinal cord (Dehnisch Ellström et al., 2019), kidney (Johnson et al., 2011), intestine (Ohno et al., 2021) and heart (Matrone et al., 2013). In bone, only few laser-assisted ablation assays have been employed. Two assays were performed in non-osseous tissues - the wound epidermis covering regenerating bone elements in fins (J. Zhang et al., 2012) and hypothalamic neurons during early development (Suarez-Bregua et al., 2017), which lead to altered fin ray patterning and mineralization defects in craniofacial bones, respectively. Substantial osteoblast ablation was performed by Chang & Franz-Odendaal in selected skeletal condensations of developing infraorbital bones in older zebrafish larvae (10 mm standard length, age > one month, (Singleman & Holtzman, 2014)). While the bones recovered, they were however smaller and aberrant in shape (Chang & Franz-Odendaal, 2014). In our assay, ablation of a maximum of 10 % of opercular osteoblasts was subcritical and did not compromise bone growth, which could also reflect the ability of younger individuals to better compensate for tissue damage during development.

Our model represents a novel approach to study bone cell turnover in homeostasis and repair. We show that ablation of only few osteoblasts is sufficient to initiate an immune cell response of graded severity, depending on how many cells were ablated initially. This is especially interesting considering that osteoblast senescence and cell death are frequent processes in bone homeostasis with osteoblasts having a relatively short life span (Manolagas, 2000). The consequences of isolated osteoblast death during homeostasis and medical treatment, as well as their replacement, are not particularly clear. In recent years, osteocytes have gained center stage as sensors of biomechanical strain and players in modeling and remodeling of bone (BONEWALD, 2007; Kennedy et al., 2012; Ru & Wang, 2020). However, osteoblasts, mirroring the pre-osteocytic cell stage, have suggested to play a similar role in sensation of

677 microscopic tissue damage. This is illustrated by the fact that anosteocytic bones undergo
678 modeling in teleost fish (medaka (Ofer et al., 2019)), which is mediated by Sclerostin levels in
679 bone lining osteoblasts, and is supported by the observation that osteocytic bones do not
680 necessarily undergo remodeling (Currey et al., 2017). Another aspect of osteoblast biology is
681 their declined performance in aged bone, which is partly mediated by accumulation of ROS
682 (H. N. Kim et al., 2018), and rising levels of glucocorticoids (M Almeida & O'Brien, 2013). Both
683 factors, which we modeled with the help of laser-assisted osteoblast ablation, influence bone
684 health directly and indirectly, by impairing osteo-immune cell communication (Ahmad et al.,
685 2019; Lean et al., 2005). While we are aware that the presented assay makes use of a growing
686 bone of simple structure, we suggest to use it to *in vivo* monitor the processes of osteoblast
687 recovery after cell death, and to study the varying contribution of immune cells to bone repair
688 and integrity. In addition, interaction of leukocyte cell types, such as the process of reverse
689 migration of neutrophils first observed in zebrafish (Mathias et al., 2006) and later
690 demonstrated in mammals (Woodfin et al., 2011), and the generation of
691 macrophage/monocyte-derived osteoclasts in response to ROS and increased stress signaling
692 can be studied. Finally, the model enables studies on the contribution of different osteoblast
693 progenitor cell pools to osteoblast recovery and can potentially be used in slightly older
694 animals to visualize the plasticity of mature osteoblasts undergoing dedifferentiation.
695
696 **Summary**
697 In conclusion, we present a comprehensive study on a new laser-assisted osteoblast ablation
698 paradigm, which enables researchers to study osteoblast – immune cell interactions *in vivo*.
699 We investigated the specific characteristics of this sterile lesion assay and show that a varying
700 number of osteoblasts can be ablated and that recovery occurs fast when 10 % of the
701 opercular osteoblasts are ablated. Using spinning disc confocal microscopy, we tracked the
702 immediate response of neutrophils and macrophages, which migrated into the site of ablation
703 at which ROS were released quickly. A significant number of recruited macrophages displayed
704 an inflammatory phenotype, which was inhibited by pharmacological glucocorticoid
705 exposure. Moreover, glucocorticoid-treatment significantly impaired macrophage migration
706 into the region of interest and affected osteoblast recovery. Ablation of *mpeg1*+ macrophages
707 impaired osteoblast repopulation of the injured area suggesting a bone-anabolic macrophage
708 function. Laser-assisted ablation of osteoblasts can be used to better understand microscopic

bone repair during tissue homeostasis and to explore the relevance of leukocyte recruitment in this process.

Material & Methods

Animal experiments

All procedures were performed in accordance with the animal handling and research regulations of the Landesdirektion Sachsen (Permit numbers AZ DD25-5131/354/87, DD25-5131/450/4, 25-5131/496/56 and amendments).

Fish lines and husbandry

The following previously described transgenic zebrafish lines were used: *osterix*:nGFP (Tg(*Ola.Sp7*:NLS-GFP)^{zf132})(Spoorendonk et al., 2008), histone Cherry (Tg(*h2afv*:h2afv-mCherry)^{tud7})(Knopf et al., 2011), *mmp9:*EGFP (TgBAC(*mmp9*:EGFP-NTR)^{tyt206})(Ando et al., 2017), mpo:GFP (Tg(BAC*mpo*:gfp)^{i114})(Renshaw et al., 2006), m*peg1:*mCherry (Tg(*mpeg1*:mCherry)^{gl23})(Ellett et al., 2011), *mpeg1:*YFP-NTR (Tg(*mpeg1*:NTR-EYFP)^{w202})(Petrie et al., 2014), TgBAC(*tnfa*:GFP)^{pd1028})(Marjoram et al., 2015), *irg1:*EGFP (Tg(*acod1*:EGFP)^{nz26})(Sanderson et al., 2015), *osterix*:CreERT2-p2a-mCherry (Tg(*Ola.sp7*:CreERT2-P2A-mCherry)^{tud8})(Knopf et al., 2011), *hsp70*:R2nlsG (Tg(*hsp70l*:loxP-DsRed2-loxP-nlsEGFP)^{tud9})(Knopf et al., 2011), *kdrl*:CFP (Tg(*kdrl*:CFP)^{zf410})(Hess & Boehm, 2012).

For creation of the *ctsK*:nlsmCherry transgenic zebrafish line a fragment containing the 4 kb promotor region and start of exon1 of the *Danio rerio cathepsin K* was cloned upstream of nlsmCherry into a pBluescript-based vector containing Tol2 transposable sites flanking the insert (kindly provided by Anke Weber and Stefan Hans). The following primers were used for amplification: ATATCCTCTCACAGGACATCAAACAGCGAAACGAG (adding an EcoNI restriction site) and TATAGGCCGGCCTGAGCAAGAAGAAATGCACC (adding a FseI restriction site). EcoNI and FseI restriction enzymes were used for cloning. A transgenic line was created by injecting the plasmid DNA with transposase mRNA into fertilized eggs. Throughout larval growth

737 transgene expression was detectable in the pharyngeal region comparable to another
738 previously published zebrafish *ctsK*-line (Sharif et al., 2014).
739 Fish were bred and maintained as described (Brand M et al., 2002).
740

741 Lesion paradigm and *in vivo* imaging

742 In order to perform osteoblast ablations, zebrafish larvae were anesthetized in 0.02 % Tricaine
743 (MS222, Merck, Taufkirchen, Germany) and embedded in 1 % Low melt agarose (LMA, Biozym
744 Scientific GmbH, Hessisch Oldendorf, Germany) in E3 in a glass bottom microwell dish (35
745 mm, 14 mm microwell, MatTek Corporation, Ashland, MA, USA). To immobilize the larvae, 20
746 µl of 0,4 % Tricaine were added to 1.5 ml LMA (final concentration 0.005 % Tricaine). They
747 were laid on the side to position the opercle region close to the glass bottom for imaging
748 accessibility. For prednisolone-treatment the larvae were kept in prednisolone (Merck,
749 Taufkirchen, Germany) or DMSO (Merck, Taufkirchen, Germany) control conditions by adding
750 autoclaved E3 with 0.01% Tricaine and 25 µM prednisolone or 0.05% DMSO to the dish after
751 the LMA had solidified, otherwise E3 with 0.01% Tricaine was added. The osteoblast lesion
752 was performed using a UV laser adjusted to the Andor spinning disk system equipped with a
753 Yokogawa CSU-X1, Zeiss AxioObserver.Z1 and an iXon+ camera facilitating simultaneous
754 imaging with LabVIEW 2009. The same laser cutter settings were used throughout the study,
755 consisting of 2.0 intensity, 20 pulses/shot, four shots/µm^2 and two shooting circles of 15 and
756 7 µm Ø. Cell death was confirmed by loss of GFP signal. Afterwards the larvae were carefully
757 removed from the LMA and kept in E3 until further imaging was performed. Non-lesioned
758 controls were mock-treated i.e. they were also anesthetized and embedded in LMA.
759 Short-term imaging was performed with LabVIEW 2009 with the setup described above, while
760 long term imaging was performed with Andor iQ2 software or a Dragonfly spinning disk
761 equipped with a sCMOS camera and Fusion software. In both imaging approaches, the same
762 laser power, gain settings and exposure times were used. Larvae were kept in LMA after the
763 lesion and were continuously imaged at different time intervals. Data were processed with
764 Image J Software version 1.53c or Arivis Vision4D version 2.12.6. and 3.3.0 where mentioned,
765 in order to obtain images and movies. For tracking of macrophages Arivis Vision4D version
766 2.12.6. was used. First, the data were filtered using a convolution enhancement filter which

was followed by drift correction using the GFP channel. Afterwards, individual macrophages were tracked using the blob finder and Brownian motion segment tracker.
Only macrophages whose complete cell bodies were visible and which very present in the field of view for more than 30 min were tracked. At the end, the tracking was manually verified, aberrant tracks were excluded and separated tracks were merged.

Drug treatments

Prednisolone treatment of zebrafish larvae was carried out as previously described (Geurtzen et al., 2017).
DPI (Diphenyleneiodonium chloride, Merck, Taufkirchen, Germany) treatment of 3 dpf zebrafish larvae before finfold resection was carried out as previously described (Robertson et al., 2016). DPI treatment on 6 dpf larvae started 5 h before laser ablation and continued throughout the live imaging period with the same concentration used on 3 dpf larvae (100 µM).
Nifupirinol (NFP) treatment was performed as previsouly described (Bergemann et al., 2018). A 2.5 mM stock solution of NFP in DMSO was prepared and stored at -20ºC. Larval zebrafish were soaked in 2.5 µM NFP for up to 6 consecutive days in the dark at 28ºC.

Fin fold resection

3 dpf larvae were anesthetized and fin fold resection was performed as previously described (Isles et al., 2019).

Staining techniques

Alizarin red staining of the live zebrafish larvae was performed as previously described (Kimmel et al., 2010). For quantification of the opercle volume the surface tool in Imaris 8.1 was used to reproduce the alizarin red stained area surface and to calculate the corresponding volume.
CellROX staining was conducted as previously described (Kulkarni et al., 2018), however, instead of CellROX green, CellROX orange (ThermoFisher Scientific, Waltham, MA, USA) was used. After staining, larvae were embedded in 1% LMA, lesioned and live imaged for 15 min.

797

798 Osteoblast fate mapping

799 *osterix*:CreERT2-p2a-mCherry, *hsp70*:R2nlsG double transgenic 5 dpf larvae were soaked in
800 10 µM 4-hydroxytamoxifen (4-OHT, Merck, Taufkirchen, Germany) or the corresponding
801 amount of vehicle control ethanol for 10 h. Larvae were lesioned at 6 dpf. One or two days
802 later (7 or 8 dpf), larvae were heat shocked once at 37°C for 1 h. Roughly 12 h post heat shock
803 the larvae were analyzed for recombination by the appearance of nlsGFP+ cells.

804

805 Quantification of GFP and mCherry expression, steromicroscopy

806 For quantification of GFP and mCherry expression post lesion the larvae were anesthetized
807 with 0.02% Tricaine (MS222) and again embedded in 1% LMA in a glass bottom dish. The
808 larvae were imaged once with an Andor Dragonfly Spinning Disk equipped with a sCMOS
809 camera. For each time point a different set off larvae was used. Identical settings for
810 magnification, exposure time, pinhole size, laser power and z-stack interval were used
811 throughout the whole experiment. Intensity measurements were conducted using the Plot
812 Profile Tool in Image J Software version 1.53c.
813 Stereomicroscopy of fin fold resected zebrafish larvae and the head region of *ctsK*:nlsmCherry
814 transgenic zebrafish was performed with the help of a Zeiss SteREO Discovery.V12 equipped
815 with a AxioCam MRm and AxioVison software version 4.7.1.0.
816

817 Image processing

818 Brightness, contrast and levels were adjusted using Adobe Photoshop CS6 and 2020 software.
819 Images were processed with identical settings using the legacy option.
820

821 Statistical analysis
822 Statistical analysis was run using GraphPad Prism 8.3.1. Unpaired two-sided t-tests with
823 Welch's correction, Tukey's multiple comparison one-way ANOVA and Sidak's multiple
824 comparison two-way ANOVA tests were performed wherever applicable.
825

826

827 **Acknowledgements**

828 We would like to thank Isabell Weber for help in establishing the laser-assisted lesion assay
829 and Michael Brand for helpful discussions. We are very grateful to Atsushi Kawakami (Tokyo,
830 Japan), Michel Bagnat (Durham, UK) and C.J. Hall (Auckland, New Zealand) for sharing
831 transgenic fish. Special thanks goes to Stefan Grill, Nicholas Chartier and Lokesh Pimpale for
832 providing access to their Spinning Disk Microscope and technical support. We would also like
833 to thank Anke Weber and Stefan Hans for sharing reagents. Our thanks also goes to the Light
834 Microscopy core facility at the Center for Molecular and Cellular Bioengineering at the TU
835 Dresden and Marika Fischer, Jitka Michling and Daniela Moegel for excellent fish care. We
836 thank Henriette Knopf for proofreading the manuscript.

837

838 **Author contributions**

839 Experiments were designed and analyzed by KG, AD and FK. KG and AD performed
840 experiments. KG and FK wrote the manuscript and accept responsibility for the integrity of
841 data analysis.

842

843 **Competing interests**

844 The authors declare no competing financial or non-financial interest.

845

846 **Funding**

847 This work was supported by the DFG Transregio 67 (project 387653785) and the DFG SPP 2084
848 µBone (project KN 1102/2-1). The work at the TU Dresden is co-financed with tax revenues
849 based on the budget agreed by the Saxonian Landtag.

850

851 **References**

852 Ahi, E. P., Walker, B. S., Lassiter, C. S., & Jónsson, Z. O. (2016). Investigation of the effects of

853 estrogen on skeletal gene expression during zebrafish larval head development. *PeerJ*,
854 *4*, e1878. https://doi.org/10.7717/PEERJ.1878

855 Ahmad, M., Hachemi, Y., Paxian, K., Mengele, F., Koenen, M., & Tuckermann, J. (2019). A
856 Jack of All Trades: Impact of Glucocorticoids on Cellular Cross-Talk in
857 Osteoimmunology. *Frontiers in Immunology*, *10*, 2460.
858 https://doi.org/10.3389/fimmu.2019.02460

859 Akiva, A., Kerschnitzki, M., Pinkas, I., Wagermaier, W., Yaniv, K., Fratzl, P., Addadi, L., &
860 Weiner, S. (2016). Mineral Formation in the Larval Zebrafish Tail Bone Occurs via an
861 Acidic Disordered Calcium Phosphate Phase. *Journal of the American Chemical Society*,
862 *138*(43), 14481–14487. https://doi.org/10.1021/jacs.6b09442

863 Alexander, K. A., Chang, M. K., Maylin, E. R., Kohler, T., Müller, R., Wu, A. C., Van Rooijen, N.,
864 Sweet, M. J., Hume, D. A., Raggatt, L. J., & Pettit, A. R. (2011). Osteal macrophages
865 promote in vivo intramembranous bone healing in a mouse tibial injury model. *Journal*
866 *of Bone and Mineral Research : The Official Journal of the American Society for Bone*
867 *and Mineral Research*, *26*(7), 1517–1532. https://doi.org/10.1002/jbmr.354

868 Almeida, M, & O'Brien, C. A. (2013). Basic Biology of Skeletal Aging: Role of Stress Response
869 Pathways. *The Journals of Gerontology Series A: Biological Sciences and Medical*
870 *Sciences*, *68*(10), 1197–1208. https://doi.org/10.1093/gerona/glt079

871 Almeida, Maria. (2012). Aging mechanisms in bone. *BoneKEy Reports*, *1*(7).
872 https://doi.org/10.1038/bonekey.2012.102

873 Ando, K., Shibata, E., Hans, S., Brand, M., & Kawakami, A. (2017). Osteoblast Production by
874 Reserved Progenitor Cells in Zebrafish Bone Regeneration and Maintenance.
875 *Developmental Cell*. https://doi.org/10.1016/j.devcel.2017.10.015

876 Andrew, J. G., Andrew, S. M., Freemont, A. J., & Marsh, D. R. (1994). Inflammatory cells in
877 normal human fracture healing. *Acta Orthopaedica Scandinavica*, *65*(4), 462–466.
878 http://www.ncbi.nlm.nih.gov/pubmed/7976298

879 Baek, K. H., Oh, K. W., Lee, W. Y., Lee, S. S., Kim, M. K., Kwon, H. S., Rhee, E. J., Han, J. H.,
880 Song, K. H., Cha, B. Y., Lee, K. W., & Kang, M. Il. (2010). Association of oxidative stress
881 with postmenopausal osteoporosis and the effects of hydrogen peroxide on osteoclast

formation in human bone marrow cell cultures. *Calcified Tissue International*, *87*(3), 226–235. https://doi.org/10.1007/s00223-010-9393-9

Bai, X.-C., Lu, D., Liu, A.-L., Zhang, Z.-M., Li, X.-M., Zou, Z.-P., Zeng, W.-S., Cheng, B.-L., & Luo, S.-Q. (2005). *Reactive Oxygen Species Stimulates Receptor Activator of NF-B Ligand Expression in Osteoblast**. https://doi.org/10.1074/jbc.M409332200

Banerji, R., Eble, D. M., Iovine, M. K., & Skibbens, R. V. (2016). Esco2 regulates *cx43* expression during skeletal regeneration in the zebrafish fin. *Developmental Dynamics*, *245*(1), 7–21. https://doi.org/10.1002/dvdy.24354

Barros-Becker, F., Lam, P.-Y., Fisher, R., & Huttenlocher, A. (2017). Live imaging reveals distinct modes of neutrophil and macrophage migration within interstitial tissues. *Journal of Cell Science*, jcs.206128. https://doi.org/10.1242/jcs.206128

Batoon, L., Millard, S. M., Wullschleger, M. E., Preda, C., Wu, A. C.-K., Kaur, S., Tseng, H.-W., Hume, D. A., Levesque, J.-P., Raggatt, L. J., & Pettit, A. R. (2017). CD169 + macrophages are critical for osteoblast maintenance and promote intramembranous and endochondral ossification during bone repair. *Biomaterials*. https://doi.org/10.1016/j.biomaterials.2017.10.033

Bergemann, D., Massoz, L., Bourdouxhe, J., Carril Pardo, C. A., Voz, M. L., Peers, B., & Manfroid, I. (2018). Nifurpirinol: A more potent and reliable substrate compared to metronidazole for nitroreductase-mediated cell ablations. *Wound Repair and Regeneration*. https://doi.org/10.1111/wrr.12633

BONEWALD, L. F. (2007). Osteocytes as Dynamic Multifunctional Cells. *Annals of the New York Academy of Sciences*, *1116*(1), 281–290. https://doi.org/10.1196/annals.1402.018

Brand M, Granato M, & Nuesslein-Volhard C. (2002). Keeping and raising zebrafish. In Nuesslein-Volhard C & Dahm R (Eds.), *Zebrafish: A Practical Approach* (pp. 7–37). Oxford University Press.

Brittijn, S. A., Duivesteijn, S. J., Belmamoune, M., Bertens, L. F. M., Bitter, W., de Bruijn, J. D., Champagne, D. L., Cuppen, E., Flik, G., Vandenbroucke-Grauls, C. M., Janssen, R. A. J., de Jong, I. M. L., de Kloet, E. R., Kros, A., Meijer, A. H., Metz, J. R., van der Sar, A. M., Schaaf, M. J. M., Schulte-Merker, S., … Richardson, M. K. (2009). Zebrafish development

and regeneration: new tools for biomedical research. *The International Journal of Developmental Biology*, *53*(5–6), 835–850. https://doi.org/10.1387/ijdb.082615sb

Buehring, B., Viswanathan, R., Binkley, N., & Busse, W. (2013). Glucocorticoid-induced osteoporosis: An update on effects and management. *Journal of Allergy and Clinical Immunology*, *132*(5), 1019–1030. https://doi.org/10.1016/J.JACI.2013.08.040

Cain, D. W., & Cidlowski, J. A. (2017). Immune regulation by glucocorticoids. *Nature Reviews Immunology*, *17*(4), 233–247. https://doi.org/10.1038/nri.2017.1

Callaway, D. A., & Jiang, J. X. (2015). Reactive oxygen species and oxidative stress in osteoclastogenesis, skeletal aging and bone diseases. In *Journal of Bone and Mineral Metabolism* (Vol. 33, Issue 4, pp. 359–370). Springer Tokyo. https://doi.org/10.1007/s00774-015-0656-4

Carvalho, F. R., Fernandes, A. R., Cancela, M. L., & Gavaia, P. J. (2017). Improved regeneration and de novo bone formation in a diabetic zebrafish model treated with paricalcitol and cinacalcet. *Wound Repair and Regeneration*, *25*(3), 432–442. https://doi.org/10.1111/wrr.12536

Chang, C. T., & Franz-Odendaal, T. A. (2014). Perturbing the developing skull: Using laser ablation to investigate the robustness of the infraorbital bones in zebrafish (Danio rerio). *BMC Developmental Biology*, *14*(1), 44. https://doi.org/10.1186/s12861-014-0044-7

Charles, J. F., & Nakamura, M. C. (2014). *Bone and the Innate Immune System*. https://doi.org/10.1007/s11914-014-0195-2

Chassot, B., Pury, D., & Jaźwińska, A. (2016). Zebrafish fin regeneration after cryoinjury-induced tissue damage. *Biology Open*, *5*(6), 819–828. https://doi.org/10.1242/bio.016865

Chatani, M., Takano, Y., & Kudo, A. (2011). Osteoclasts in bone modeling, as revealed by in vivo imaging, are essential for organogenesis in fish. *Developmental Biology*, *360*(1), 96–109. https://doi.org/10.1016/j.ydbio.2011.09.013

Chatzopoulou, A., Heijmans, J. P. M., Burgerhout, E., Oskam, N., Spaink, H. P., Meijer, A. H.,

939 & Schaaf, M. J. M. (2016). Glucocorticoid-Induced Attenuation of the Inflammatory
940 Response in Zebrafish. *Endocrinology*, *157*(7), 2772–2784.
941 https://doi.org/10.1210/en.2015-2050

942 Chazaud, B. (2014). Macrophages: Supportive cells for tissue repair and regeneration.
943 *Immunobiology*, *219*(3), 172–178. https://doi.org/10.1016/j.imbio.2013.09.001

944 Chen, A. T., & Zon, L. I. (2009). Zebrafish blood stem cells. *Journal of Cellular Biochemistry*,
945 *108*(1), 35–42. https://doi.org/10.1002/jcb.22251

946 Cox, B. D., De Simone, A., Tornini, V. A., Singh, S. P., Di Talia, S., & Poss, K. D. (2018). In Toto
947 Imaging of Dynamic Osteoblast Behaviors in Regenerating Skeletal Bone. *Current*
948 *Biology*, *28*(24), 3937-3947.e4. https://doi.org/10.1016/J.CUB.2018.10.052

949 Cubbage, C. C., & Mabee, P. M. (1996). Development of the cranium and paired fins in the
950 zebrafishDanio rerio (Ostariophysi, Cyprinidae). *Journal of Morphology*, *229*(2), 121–
951 160. https://doi.org/10.1002/(SICI)1097-4687(199608)229:2<121::AID-
952 JMOR1>3.0.CO;2-4

953 Curado, S., Stainier, D. Y. R., & Anderson, R. M. (2008). Nitroreductase-mediated cell/tissue
954 ablation in zebrafish: a spatially and temporally controlled ablation method with
955 applications in developmental and regeneration studies. *Nature Protocols*, *3*(6), 948–
956 954. https://doi.org/10.1038/nprot.2008.58

957 Currey, J. D., Dean, M. N., & Shahar, R. (2017). Revisiting the links between bone
958 remodelling and osteocytes: insights from across phyla. *Biological Reviews*, *92*(3),
959 1702–1719. https://doi.org/10.1111/brv.12302

960 Dallas, S. L., & Moore, D. S. (2020). Using confocal imaging approaches to understand the
961 structure and function of osteocytes and the lacunocanalicular network. In *Bone* (Vol.
962 138, p. 115463). Elsevier Inc. https://doi.org/10.1016/j.bone.2020.115463

963 Dallas, S. L., Veno, P. A., & Tiede-Lewis, L. A. M. (2019). Live cell imaging of bone cell and
964 organ cultures. In *Methods in Molecular Biology* (Vol. 1914, pp. 467–506). Humana
965 Press Inc. https://doi.org/10.1007/978-1-4939-8997-3_27

966 Davies, L. C., Jenkins, S. J., Allen, J. E., & Taylor, P. R. (2013). Tissue-resident macrophages. In

Nature Immunology (Vol. 14, Issue 10, pp. 986–995). Nature Publishing Group. https://doi.org/10.1038/ni.2705

De Simone, A., Evanitsky, M. N., Hayden, L., Cox, B. D., Wang, J., Tornini, V. A., Ou, J., Chao, A., Poss, K. D., & Di Talia, S. (2021). Control of osteoblast regeneration by a train of Erk activity waves. *Nature*, *590*(7844), 129. https://doi.org/10.1038/s41586-020-03085-8

Debnath, S., Yallowitz, A. R., McCormick, J., Lalani, S., Zhang, T., Xu, R., Li, N., Liu, Y., Yang, Y. S., Eiseman, M., Shim, J. H., Hameed, M., Healey, J. H., Bostrom, M. P., Landau, D. A., & Greenblatt, M. B. (2018). Discovery of a periosteal stem cell mediating intramembranous bone formation. *Nature*, *562*(7725), 133–139. https://doi.org/10.1038/s41586-018-0554-8

Dehnisch Ellström, I., Spulber, S., Hultin, S., Norlin, N., Ceccatelli, S., Hultling, C., & Uhlén, P. (2019). Spinal cord injury in zebrafish induced by near-infrared femtosecond laser pulses. *Journal of Neuroscience Methods*, *311*, 259–266. https://doi.org/10.1016/j.jneumeth.2018.10.035

DeLaurier, A., Alvarez, C. L., & Wiggins, K. J. (2019). hdac4 mediates perichondral ossification and pharyngeal skeleton development in the zebrafish. *PeerJ*, *7*, e6167. https://doi.org/10.7717/peerj.6167

Dempster, D. (2006). Anatomy and functions of the adult skeleton. *Primer of the Metabolic Bone Diseases and Disorders of Mineral Metabolism*. http://www.homepages.ucl.ac.uk/~ucgatma/Anat3048/PAPERS etc/ASBMR Primer Ed 6/Ch 1-7 - Morphogenesis, Structure & Cell Biology of Bone.pdf

Demy, D. Lou, Tauzin, M., Lancino, M., Le Cabec, V., Redd, M., Murayama, E., Maridonneau-Parini, I., Trede, N., & Herbomel, P. (2017). Trim33 is essential for macrophage and neutrophil mobilization to developmental or inflammatory cues. *Journal of Cell Science*, *130*(17), 2797–2807. https://doi.org/10.1242/jcs.203471

den Uyl, D., Bultink, I. E. M., & Lems, W. F. (2011). Glucocorticoid-induced osteoporosis. *Clinical and Experimental Rheumatology*, *29*(5 Suppl 68), S93-8. http://www.ncbi.nlm.nih.gov/pubmed/22018192

Diez-Roux, G., & Lang, R. A. (1997). Macrophages induce apoptosis in normal cells in vivo.

Development, *124*(18), 3633–3638.

Domazetovic, V. (2017). Oxidative stress in bone remodeling: role of antioxidants. *Clinical Cases in Mineral and Bone Metabolism*, *14*(2), 209. https://doi.org/10.11138/ccmbm/2017.14.1.209

Du, S. J., Frenkel, V., Kindschi, G., & Zohar, Y. (2001). Visualizing Normal and Defective Bone Development in Zebrafish Embryos Using the Fluorescent Chromophore Calcein. *Developmental Biology*, *238*(2), 239–246. https://doi.org/10.1006/dbio.2001.0390

Duffield, J. S. (2003). The inflammatory macrophage: a story of Jekyll and Hyde. *Clinical Science (London, England : 1979)*, *104*(1), 27–38. https://doi.org/10.1042/

Ellett, F., & Lieschke, G. J. (2010). Zebrafish as a model for vertebrate hematopoiesis. *Current Opinion in Pharmacology*, *10*(5), 563–570. https://doi.org/10.1016/J.COPH.2010.05.004

Ellett, F., Pase, L., Hayman, J. W., Andrianopoulos, A., & Lieschke, G. J. (2011). mpeg1 promoter transgenes direct macrophage-lineage expression in zebrafish. *Blood*, *117*(4), e49-56. https://doi.org/10.1182/blood-2010-10-314120

Feng, X., & McDonald, J. M. (2011). Disorders of bone remodeling. *Annual Review of Pathology*, *6*, 121–145. https://doi.org/10.1146/annurev-pathol-011110-130203

Feng, Y., Santoriello, C., Mione, M., Hurlstone, A., & Martin, P. (2010). Live Imaging of Innate Immune Cell Sensing of Transformed Cells in Zebrafish Larvae: Parallels between Tumor Initiation and Wound Inflammation. *PLoS Biology*, *8*(12), e1000562. https://doi.org/10.1371/journal.pbio.1000562

Fiedler, I. A. K., Schmidt, F. N., Wölfel, E. M., Plumeyer, C., Milovanovic, P., Gioia, R., Tonelli, F., Bale, H. A., Jähn, K., Besio, R., Forlino, A., & Busse, B. (2018). Severely Impaired Bone Material Quality in Chihuahua Zebrafish Resembles Classical Dominant Human Osteogenesis Imperfecta. *Journal of Bone and Mineral Research*, *33*(8), 1489–1499. https://doi.org/10.1002/jbmr.3445

Formella, I., Svahn, A. J., Radford, R. A. W., Don, E. K., Cole, N. J., Hogan, A., Lee, A., Chung, R. S., & Morsch, M. (2018). Real-time visualization of oxidative stress-mediated

neurodegeneration of individual spinal motor neurons in vivo. *Redox Biology*, *19*, 226–234. https://doi.org/10.1016/j.redox.2018.08.011

Fraser, L.-A., & Adachi, J. D. (2009). Glucocorticoid-induced osteoporosis: treatment update and review. *Therapeutic Advances in Musculoskeletal Disease*, *1*(2), 71–85. https://doi.org/10.1177/1759720X09343729

Furuya, M., Kikuta, J., Fujimori, S., Seno, S., Maeda, H., Shirazaki, M., Uenaka, M., Mizuno, H., Iwamoto, Y., Morimoto, A., Hashimoto, K., Ito, T., Isogai, Y., Kashii, M., Kaito, T., Ohba, S., Chung, U. Il, Lichtler, A. C., Kikuchi, K., … Ishii, M. (2018). Direct cell-cell contact between mature osteoblasts and osteoclasts dynamically controls their functions in vivo. *Nature Communications*, *9*(1), 1–12. https://doi.org/10.1038/s41467-017-02541-w

Gauron, C., Rampon, C., Bouzaffour, M., Ipendey, E., Teillon, J., Volovitch, M., & Vriz, S. (2013). Sustained production of ROS triggers compensatory proliferation and is required for regeneration to proceed. *Scientific Reports*, *3*(1), 1–9. https://doi.org/10.1038/srep02084

Geurtzen, K., Knopf, F., Wehner, D., Huitema, L. F. A., Schulte-Merker, S., & Weidinger, G. (2014). Mature osteoblasts dedifferentiate in response to traumatic bone injury in the zebrafish fin and skull. *Development*, *141*(11), 2225–2234. https://doi.org/10.1242/DEV.105817

Geurtzen, K., Vernet, A., Freidin, A., Rauner, M., Hofbauer, L. C., Schneider, J. E., Brand, M., & Knopf, F. (2017). Immune Suppressive and Bone Inhibitory Effects of Prednisolone in Growing and Regenerating Zebrafish Tissues. *Journal of Bone and Mineral Research*, *32*(12), 2476–2488. https://doi.org/10.1002/jbmr.3231

Gistelinck, C., Kwon, R. Y., Malfait, F., Symoens, S., Harris, M. P., Henke, K., Hawkins, M. B., Fisher, S., Sips, P., Guillemyn, B., Bek, J. W., Vermassen, P., De Saffel, H., Witten, P. E., Weis, M. A., De Paepe, A., Eyre, D. R., Willaert, A., & Coucke, P. J. (2018). Zebrafish type I collagen mutants faithfully recapitulate human type I collagenopathies. *Proceedings of the National Academy of Sciences of the United States of America*, *115*(34), E8037–E8046. https://doi.org/10.1073/pnas.1722200115

1053 Gray, C., Loynes, C. A., Whyte, M. K. B., Crossman, D. C., Renshaw, S. A., & Chico, T. J. A.
1054 (2011). Simultaneous intravital imaging of macrophage and neutrophil behaviour
1055 during inflammation using a novel transgenic zebrafish. *Thrombosis and Haemostasis*,
1056 *105*(5), 811–819. https://doi.org/10.1160/TH10-08-0525

1057 Gurevich, D. B., Severn, C. E., Twomey, C., Greenhough, A., Cash, J., Toye, A. M., Mellor, H.,
1058 & Martin, P. (2018). Live imaging of wound angiogenesis reveals macrophage
1059 orchestrated vessel sprouting and regression. *The EMBO Journal*, *37*(13), e97786.
1060 https://doi.org/10.15252/embj.201797786

1061 Hachemi, Y., Rapp, A. E., Picke, A.-K., Weidinger, G., Ignatius, A., & Tuckermann, J. (2018).
1062 Molecular mechanisms of glucocorticoids on skeleton and bone regeneration after
1063 fracture. *Journal of Molecular Endocrinology*, *61*(1), R75–R90.
1064 https://doi.org/10.1530/JME-18-0024

1065 Hall, C., Flores, M. V., Chien, A., Davidson, A., Crosier, K., & Crosier, P. (2009). Transgenic
1066 zebrafish reporter lines reveal conserved Toll-like receptor signaling potential in
1067 embryonic myeloid leukocytes and adult immune cell lineages. *Journal of Leukocyte*
1068 *Biology*, *85*(5), 751–765. https://doi.org/10.1189/jlb.0708405

1069 Hall, C., Flores, M. V., Storm, T., Crosier, K., & Crosier, P. (2007). The zebrafish lysozyme C
1070 promoter drives myeloid-specific expression in transgenic fish. *BMC Developmental*
1071 *Biology*, *7*, 42. https://doi.org/10.1186/1471-213X-7-42

1072 Hall, C. J., Boyle, R. H., Astin, J. W., Flores, M. V., Oehlers, S. H., Sanderson, L. E., Ellett, F.,
1073 Lieschke, G. J., Crosier, K. E., & Crosier, P. S. (2013). Immunoresponsive gene 1
1074 augments bactericidal activity of macrophage-lineage cells by regulating β-oxidation-
1075 dependent mitochondrial ros production. *Cell Metabolism*, *18*(2), 265–278.
1076 https://doi.org/10.1016/j.cmet.2013.06.018

1077 Hall, C. J., Boyle, R. H., Sun, X., Wicker, S. M., Misa, J. P., Krissansen, G. W., Print, C. G.,
1078 Crosier, K. E., & Crosier, P. S. (2014). Epidermal cells help coordinate leukocyte
1079 migration during inflammation through fatty acid-fuelled matrix metalloproteinase
1080 production. *Nature Communications*, *5*, 3880. https://doi.org/10.1038/ncomms4880

1081 Hammond, C. L., & Moro, E. (2012). Using transgenic reporters to visualize bone and

1082 cartilage signaling during development in vivo. *Frontiers in Endocrinology*, *3*, 91.
1083 https://doi.org/10.3389/fendo.2012.00091

1084 Hans, S., Kaslin, J., Freudenreich, D., & Brand, M. (2009). Temporally-controlled site-specific
1085 recombination in zebrafish. *PLoS ONE*, *4*(2).
1086 https://doi.org/10.1371/journal.pone.0004640

1087 Hasegawa, Tetsuo, Kikuta, J., & Ishii, M. (2019). Imaging the bone-immune cell interaction in
1088 bone destruction. *Frontiers in Immunology*, *10*(MAR), 596.
1089 https://doi.org/10.3389/fimmu.2019.00596

1090 Hasegawa, Tomoya, Hall, C. J., Crosier, P. S., Abe, G., Kawakami, K., Kudo, A., & Kawakami, A.
1091 (2017). Transient inflammatory response mediated by interleukin-1β is required for
1092 proper regeneration in zebrafish fin fold. *ELife*, *6*. https://doi.org/10.7554/eLife.22716

1093 Hashimoto, K., Kaito, T., Kikuta, J., & Ishii, M. (2020). Intravital imaging of orthotopic and
1094 ectopic bone. In *Inflammation and Regeneration* (Vol. 40, Issue 1, p. 26). BioMed
1095 Central Ltd. https://doi.org/10.1186/s41232-020-00135-6

1096 Hayes, A. J., Reynolds, S., Nowell, M. A., Meakin, L. B., Habicher, J., Ledin, J., Bashford, A.,
1097 Caterson, B., & Hammond, C. L. (2013). Spinal deformity in aged zebrafish is
1098 accompanied by degenerative changes to their vertebrae that resemble osteoarthritis.
1099 *PloS One*, *8*(9), e75787. https://doi.org/10.1371/journal.pone.0075787

1100 Hazelrigg, T., Liu, N., Hong, Y., & Wang, S. (1998). *GFP Expression in Drosophila Tissues: Time*
1101 *Requirements for Formation of a Fluorescent Product*.

1102 He, M., Halima, M., Xie, Y., Schaaf, M. J. M., Meijer, A. H., & Wang, M. (2020). Ginsenoside
1103 Rg1 Acts as a Selective Glucocorticoid Receptor Agonist with Anti-Inflammatory Action
1104 without Affecting Tissue Regeneration in Zebrafish Larvae. *Cells*, *9*(5), 1107.
1105 https://doi.org/10.3390/cells9051107

1106 Herbomel, P., Thisse, B., & Thisse, C. (2001). Zebrafish Early Macrophages Colonize Cephalic
1107 Mesenchyme and Developing Brain, Retina, and Epidermis through a M-CSF Receptor-
1108 Dependent Invasive Process. *Developmental Biology*, *238*(2), 274–288.
1109 https://doi.org/10.1006/DBIO.2001.0393

1110 Hess, I., & Boehm, T. (2012). Intravital Imaging of Thymopoiesis Reveals Dynamic Lympho-
1111 Epithelial Interactions. *Immunity*, *36*(2), 298–309.
1112 https://doi.org/10.1016/j.immuni.2011.12.016

1113 Horwood, N. J. (2016). Macrophage Polarization and Bone Formation: A review. *Clinical*
1114 *Reviews in Allergy & Immunology*, *51*(1), 79–86. https://doi.org/10.1007/s12016-015-
1115 8519-2

1116 Hu, B. bing, Chen, M., Huang, R. chen, Huang, Y. bin, Xu, Y., Yin, W., Li, L., & Hu, B. (2018). In
1117 vivo imaging of mauthner axon regeneration, remyelination and synapses re-
1118 establishment after laser axotomy in zebrafish larvae. *Experimental Neurology*, *300*,
1119 67–73. https://doi.org/10.1016/j.expneurol.2017.10.028

1120 Huang, C., Ness, V. P., Yang, X., Chen, H., Luo, J., Brown, E. B., & Zhang, X. (2015).
1121 Spatiotemporal Analyses of Osteogenesis and Angiogenesis via Intravital Imaging in
1122 Cranial Bone Defect Repair. *Journal of Bone and Mineral Research*, *30*(7), 1217–1230.
1123 https://doi.org/10.1002/jbmr.2460

1124 Huemer, K., Squirrell, J. M., Swader, R., Lebert, D. C., Huttenlocher, A., & Eliceiri, K. W.
1125 (2017). ZWEDGI: Wounding and Entrapment Device for Imaging Live Zebrafish Larvae.
1126 *Zebrafish*, *14*(1), 42–50. https://doi.org/10.1089/zeb.2016.1323

1127 Ishii, M., Egen, J. G., Klauschen, F., Meier-Schellersheim, M., Saeki, Y., Vacher, J., Proia, R. L.,
1128 & Germain, R. N. (2009). Sphingosine-1-phosphate mobilizes osteoclast precursors and
1129 regulates bone homeostasis. *Nature*, *458*(7237), 524–528.
1130 https://doi.org/10.1038/nature07713

1131 Ishii, M., Fujimori, S., Kaneko, T., & Kikuta, J. (2013). Dynamic live imaging of bone: Opening
1132 a new era with “bone histodynametry.” *Journal of Bone and Mineral Metabolism*,
1133 *31*(5), 507–511. https://doi.org/10.1007/s00774-013-0437-x

1134 Ishii, M., Kikuta, J., Shimazu, Y., Meier-Schellersheim, M., & Germain, R. N. (2010).
1135 Chemorepulsion by blood S1P regulates osteoclast precursor mobilization and bone
1136 remodeling in vivo. *Journal of Experimental Medicine*, *207*(13), 2793–2798.
1137 https://doi.org/10.1084/jem.20101474

1138 Isles, H. M., Herman, K. D., Robertson, A. L., Loynes, C. A., Prince, L. R., Elks, P. M., &

1139 Renshaw, S. A. (2019). The CXCL12/CXCR4 Signaling Axis Retains Neutrophils at
1140 Inflammatory Sites in Zebrafish. *Frontiers in Immunology*, *10*, 1784.
1141 https://doi.org/10.3389/fimmu.2019.01784

1142 Jagadeeswaran, P., Paris, R., & Rao, P. (2006). Laser-induced thrombosis in zebrafish larvae:
1143 a novel genetic screening method for thrombosis. *Methods in Molecular Medicine*, *129*,
1144 187–195. https://doi.org/10.1385/1-59745-213-0:187

1145 Jamal Uddin, M., Joe, Y., Kim, S.-K., Oh Jeong, S., Ryter, S. W., Pae, H.-O., & Chung, H. T.
1146 (2016). IRG1 induced by heme oxygenase-1/carbon monoxide inhibits LPS-mediated
1147 sepsis and pro-inflammatory cytokine production. *Cellular & Molecular Immunology*,
1148 *13*(2), 170–179. https://doi.org/10.1038/cmi.2015.02

1149 Javidan, Y., & Schilling, T. F. (2004). Development of cartilage and bone. *Methods in Cell*
1150 *Biology*, *76*, 415–436. http://www.ncbi.nlm.nih.gov/pubmed/15602885

1151 Jelcic, M., Enyedi, B., Xavier, J. B., & Niethammer, P. (2017). Image-Based Measurement of
1152 H2O2 Reaction-Diffusion in Wounded Zebrafish Larvae. *Biophysical Journal*, *112*(9),
1153 2011–2018. https://doi.org/10.1016/j.bpj.2017.03.021

1154 Jilka, R. L., Weinstein, R. S., Parfitt, A. M., & Manolagas, S. C. (2007). Perspective:
1155 Quantifying Osteoblast and Osteocyte Apoptosis: Challenges and Rewards. *Journal of*
1156 *Bone and Mineral Research*, *22*(10), 1492–1501. https://doi.org/10.1359/jbmr.070518

1157 Johnson, C. S., Holzemer, N. F., & Wingert, R. A. (2011). Laser ablation of the zebrafish
1158 pronephros to study renal epithelial regeneration. *Journal of Visualized Experiments :*
1159 *JoVE*, *54*, 2845. https://doi.org/10.3791/2845

1160 Kaufmann, A., Mickoleit, M., Weber, M., & Huisken, J. (2012). Multilayer mounting enables
1161 long-term imaging of zebrafish development in a light sheet microscope. *Development*
1162 *(Cambridge)*, *139*(17), 3242–3247. https://doi.org/10.1242/dev.082586

1163 Keightley, M.-C., Wang, C.-H., Pazhakh, V., & Lieschke, G. J. (2014). Delineating the roles of
1164 neutrophils and macrophages in zebrafish regeneration models. *The International*
1165 *Journal of Biochemistry & Cell Biology*, *56*, 92–106.
1166 https://doi.org/10.1016/j.biocel.2014.07.010

1167 Kennedy, O. D., Herman, B. C., Laudier, D. M., Majeska, R. J., Sun, H. B., & Schaffler, M. B.
1168 (2012). Activation of resorption in fatigue-loaded bone involves both apoptosis and
1169 active pro-osteoclastogenic signaling by distinct osteocyte populations. *Bone*, *50*(5),
1170 1115–1122. https://doi.org/10.1016/j.bone.2012.01.025

1171 Kikuta, J., Kawamura, S., Okiji, F., Shirazaki, M., Sakai, S., Saito, H., & Ishii, M. (2013).
1172 Sphingosine-1-phosphate-mediated osteoclast precursor monocyte migration is a
1173 critical point of control in antibone-resorptive action of active vitamin D. *Proceedings of*
1174 *the National Academy of Sciences of the United States of America*, *110*(17), 7009–7013.
1175 https://doi.org/10.1073/pnas.1218799110

1176 Kim, H. N., Iyer, S., Ring, R., & Almeida, M. (2018). The Role of FoxOs in Bone Health and
1177 Disease. In *Current Topics in Developmental Biology* (Vol. 127, pp. 149–163). Academic
1178 Press Inc. https://doi.org/10.1016/bs.ctdb.2017.10.004

1179 Kim, J., & Bixel, M. G. (2020). Intravital Multiphoton Imaging of the Bone and Bone Marrow
1180 Environment. *Cytometry Part A*, *97*(5), 496–503. https://doi.org/10.1002/cyto.a.23937

1181 Kimmel, C. B., DeLaurier, A., Ullmann, B., Dowd, J., & McFadden, M. (2010). Modes of
1182 developmental outgrowth and shaping of a craniofacial bone in zebrafish. *PloS One*,
1183 *5*(3), e9475. https://doi.org/10.1371/journal.pone.0009475

1184 Klein-Nulend, J., & Bakker, A. D. (2007). Osteocytes: Mechanosensors of bone and
1185 orchestrators of mechanical adaptation. In *Clinical Reviews in Bone and Mineral*
1186 *Metabolism* (Vol. 5, Issue 4, pp. 195–209). Springer. https://doi.org/10.1007/s12018-
1187 008-9014-6

1188 Knopf, F., Hammond, C., Chekuru, A., Kurth, T., Hans, S., Weber, C. W., Mahatma, G., Fisher,
1189 S., Brand, M., Schulte-Merker, S., & Weidinger, G. (2011). Bone Regenerates via
1190 Dedifferentiation of Osteoblasts in the Zebrafish Fin. *Developmental Cell*, *20*(5), 713–
1191 724. https://doi.org/10.1016/j.devcel.2011.04.014

1192 Kolaczkowska, E., & Kubes, P. (2013). Neutrophil recruitment and function in health and
1193 inflammation. In *Nature Reviews Immunology* (Vol. 13, Issue 3, pp. 159–175). Nature
1194 Publishing Group. https://doi.org/10.1038/nri3399

1195 Kulkarni, A. A., Conteh, A. M., Sorrell, C. A., Mirmira, A., Tersey, S. A., Mirmira, R. G.,

1196 Linnemann, A. K., & Anderson, R. M. (2018). An In Vivo Zebrafish Model for
1197 Interrogating ROS-Mediated Pancreatic β-Cell Injury, Response, and Prevention.
1198 *Oxidative Medicine and Cellular Longevity*, *2018*, 1324739.
1199 https://doi.org/10.1155/2018/1324739

1200 Le Guyader, D., Redd, M. J., Colucci-Guyon, E., Murayama, E., Kissa, K., rie Briolat, V.,
1201 Mordelet, E., Zapata, A., Shinomiya, H., & Herbomel, P. (2008). *Origins and*
1202 *unconventional behavior of neutrophils in developing zebrafish*.
1203 https://doi.org/10.1182/2007

1204 Lean, J. M., Jagger, C. J., Kirstein, B., Fuller, K., & Chambers, T. J. (2005). Hydrogen peroxide
1205 is essential for estrogen-deficiency bone loss and osteoclast formation. *Endocrinology*,
1206 *146*(2), 728–735. https://doi.org/10.1210/en.2004-1021

1207 LeBert, D. C., & Huttenlocher, A. (2014). Inflammation and wound repair. *Seminars in*
1208 *Immunology*, *26*(4), 315–320. https://doi.org/10.1016/j.smim.2014.04.007

1209 LeBert, D. C., Squirrell, J. M., Rindy, J., Broadbridge, E., Lui, Y., Zakrzewska, A., Eliceiri, K. W.,
1210 Meijer, A. H., & Huttenlocher, A. (2015). Matrix metalloproteinase 9 modulates
1211 collagen matrices and wound repair. *Development (Cambridge)*, *142*(12), 2136–2146.
1212 https://doi.org/10.1242/dev.121160

1213 Lee, N. K., Choi, Y. G., Baik, J. Y., Han, S. Y., Jeong, D. W., Bae, Y. S., Kim, N., & Lee, S. Y.
1214 (2005). A crucial role for reactive oxygen species in RANKL-induced osteoclast
1215 differentiation. *Blood*, *106*(3), 852–859. https://doi.org/10.1182/blood-2004-09-3662

1216 Leibovich, S. J., & Ross, R. (1975). The role of the macrophage in wound repair. A study with
1217 hydrocortisone and antimacrophage serum. In *American Journal of Pathology* (Vol. 78,
1218 Issue 1).

1219 Lewis, G. M., & Kucenas, S. (2013). Motor nerve transection and time-lapse imaging of glial
1220 cell behaviors in live zebrafish. *Journal of Visualized Experiments : JoVE*, *76*, 50621.
1221 https://doi.org/10.3791/50621

1222 Li, L., Yan, B., Shi, Y.-Q., Zhang, W.-Q., & Wen, Z.-L. (2012). Live imaging reveals differing
1223 roles of macrophages and neutrophils during zebrafish tail fin regeneration. *The Journal*
1224 *of Biological Chemistry*, *287*(30), 25353–25360.

https://doi.org/10.1074/jbc.M112.349126

Lieschke, G. J., Oates, A. C., Crowhurst, M. O., Ward, A. C., & Layton, J. E. (2001). Morphologic and functional characterization of granulocytes and macrophages in embryonic and adult zebrafish. *Blood*, *98*(10), 3087–3096. https://doi.org/10.1182/BLOOD.V98.10.3087

Lu, P. N., Moreland, T., Christian, C. J., Lund, T. C., Steet, R. A., & Flanagan-Steet, H. (2020). Inappropriate cathepsin K secretion promotes its enzymatic activation driving heart and valve malformation. *JCI Insight*, *5*(20). https://doi.org/10.1172/jci.insight.133019

Manolagas, S. C. (2000). Birth and Death of Bone Cells: Basic Regulatory Mechanisms and Implications for the Pathogenesis and Treatment of Osteoporosis [1]. *Endocrine Reviews*, *21*(2), 115–137. https://doi.org/10.1210/edrv.21.2.0395

Marí-Beffa, M., Santamaría, J. A., Murciano, C., Santos-Ruiz, L., Andrades, J. A., Guerado, E., & Becerra, J. (2007). Zebrafish fins as a model system for skeletal human studies. *TheScientificWorldJournal*, *7*, 1114–1127. https://doi.org/10.1100/tsw.2007.190

Marjoram, L., Alvers, A., Deerhake, M. E., Bagwell, J., Mankiewicz, J., Cocchiaro, J. L., Beerman, R. W., Willer, J., Sumigray, K. D., Katsanis, N., Tobin, D. M., Rawls, J. F., Goll, M. G., & Bagnat, M. (2015). Epigenetic control of intestinal barrier function and inflammation in zebrafish. *Proceedings of the National Academy of Sciences of the United States of America*, *112*(9), 2770–2775. https://doi.org/10.1073/pnas.1424089112

Marsell, R., & Einhorn, T. A. (2011). The biology of fracture healing. *Injury*, *42*(6), 551–555. https://doi.org/10.1016/j.injury.2011.03.031

Martins, R. R., Ellis, P. S., MacDonald, R. B., Richardson, R. J., & Henriques, C. M. (2019). Resident Immunity in Tissue Repair and Maintenance: The Zebrafish Model Coming of Age. *Frontiers in Cell and Developmental Biology*, *7*, 12. https://doi.org/10.3389/fcell.2019.00012

Mateus, R., Pereira, T., Sousa, S., de Lima, J. E., Pascoal, S., Saúde, L., & Jacinto, A. (2012). In Vivo Cell and Tissue Dynamics Underlying Zebrafish Fin Fold Regeneration. *PLoS ONE*, *7*(12), e51766. https://doi.org/10.1371/journal.pone.0051766

1254 Mathew, L. K., Sengupta, S., Kawakami, A., Andreasen, E. A., Löhr, C. V, Loynes, C. A.,
1255 Renshaw, S. A., Peterson, R. T., & Tanguay, R. L. (2007). Unraveling tissue regeneration
1256 pathways using chemical genetics. *The Journal of Biological Chemistry*, *282*(48), 35202–
1257 35210. https://doi.org/10.1074/jbc.M706640200

1258 Mathias, J. R., Dodd, M. E., Walters, K. B., Yoo, S. K., Ranheim, E. A., & Huttenlocher, A.
1259 (2009). Characterization of zebrafish larval inflammatory macrophages. *Developmental*
1260 *and Comparative Immunology*, *33*(11), 1212–1217.
1261 https://doi.org/10.1016/j.dci.2009.07.003

1262 Mathias, J. R., Perrin, B. J., Liu, T.-X., Kanki, J., Look, A. T., & Huttenlocher, A. (2006).
1263 Resolution of inflammation by retrograde chemotaxis of neutrophils in transgenic
1264 zebrafish. *Journal of Leukocyte Biology*, *80*(6), 1281–1288.
1265 https://doi.org/10.1189/jlb.0506346

1266 Matrone, G., Taylor, J. M., Wilson, K. S., Baily, J., Love, G. D., Girkin, J. M., Mullins, J. J.,
1267 Tucker, C. S., & Denvir, M. A. (2013). Laser-targeted ablation of the zebrafish embryonic
1268 ventricle: A novel model of cardiac injury and repair. *International Journal of*
1269 *Cardiology*, *168*(4), 3913–3919. https://doi.org/10.1016/j.ijcard.2013.06.063

1270 Matsubara, M., Girard, M. T., Kublin, C. L., Cintron, C., & Fini, M. E. (1991). Differential roles
1271 for two gelatinolytic enzymes of the matrix metalloproteinase family in the remodelling
1272 cornea. *Developmental Biology*, *147*(2), 425–439. https://doi.org/10.1016/0012-
1273 1606(91)90300-R

1274 McColl, A., Michlewska, S., Dransfield, I., & Rossi, A. G. (2007). Effects of Glucocorticoids on
1275 Apoptosis and Clearance of Apoptotic Cells. *The Scientific World Journal*, *7*, 1165–1181.
1276 https://doi.org/10.1100/TSW.2007.224

1277 Mcdonald, G. L. K., Wang, M., Hammond, C. L., Bergen, D. J. M., Brennan, C., & Torres-Perez,
1278 J. V. (2021). *Pharmacological Manipulation of Early Zebrafish Skeletal Development*
1279 *Shows an Important Role for Smad9 in Control of Skeletal Progenitor Populations*.
1280 https://doi.org/10.3390/biom11020277

1281 McNulty, M. S., Bedell, V. M., Greenwood, T. M., Craig, T. A., Ekker, S. C., & Kumar, R. (2012).
1282 Expression of sclerostin in the developing zebrafish (Danio rerio) brain and skeleton.

Gene Expression Patterns : GEP, *12*(7–8), 228–235. https://doi.org/10.1016/j.gep.2012.04.003

McWhorter, F. Y., Wang, T., Nguyen, P., Chung, T., & Liu, W. F. (2013). Modulation of macrophage phenotype by cell shape. *Proceedings of the National Academy of Sciences of the United States of America*, *110*(43), 17253–17258. https://doi.org/10.1073/pnas.1308887110

Mitchell, R. E., Huitema, L. F. A., Skinner, R. E. H., Brunt, L. H., Severn, C., Schulte-Merker, S., & Hammond, C. L. (2013). New tools for studying osteoarthritis genetics in zebrafish. *Osteoarthritis and Cartilage*, *21*(2), 269–278. https://doi.org/10.1016/j.joca.2012.11.004

Morsch, M., Radford, R. A. W., Don, E. K., Lee, A., Hortle, E., Cole, N. J., & Chung, R. S. (2017). Triggering cell stress and death using conventional UV laser confocal microscopy. *Journal of Visualized Experiments*, *2017*(120). https://doi.org/10.3791/54983

Mosser, D. M., & Edwards, J. P. (2008). Exploring the full spectrum of macrophage activation. *Nature Reviews. Immunology*, *8*(12), 958–969. https://doi.org/10.1038/nri2448

Nguyen-Chi, M., Laplace-Builhé, B., Travnickova, J., Luz-Crawford, P., Tejedor, G., Lutfalla, G., Kissa, K., Jorgensen, C., & Djouad, F. (2017). TNF signaling and macrophages govern fin regeneration in zebrafish larvae. *Cell Death & Disease*, *8*(8), e2979. https://doi.org/10.1038/cddis.2017.374

Nguyen-Chi, M., Laplace-Builhe, B., Travnickova, J., Luz-Crawford, P., Tejedor, G., Phan, Q. T., Duroux-Richard, I., Levraud, J.-P., Kissa, K., Lutfalla, G., Jorgensen, C., & Djouad, F. (2015). Identification of polarized macrophage subsets in zebrafish. *ELife*, *4*, e07288. https://doi.org/10.7554/eLife.07288

Niethammer, P., Grabher, C., Look, A. T., & Mitchison, T. J. (2009). A tissue-scale gradient of hydrogen peroxide mediates rapid wound detection in zebrafish. *Nature*, *459*(7249), 996–999. https://doi.org/10.1038/nature08119

Novak, M. L., & Koh, T. J. (2013). Macrophage phenotypes during tissue repair. *Journal of Leukocyte Biology*, *93*(6), 875–881. https://doi.org/10.1189/jlb.1012512

1312 O'Brien, G. S., Rieger, S., Wang, F., Smolen, G. A., Gonzalez, R. E., Buchanan, J., & Sagasti, A.
1313 (2012). Coordinate development of skin cells and cutaneous sensory axons in zebrafish.
1314 *Journal of Comparative Neurology*, *520*(4), 816–831.
1315 https://doi.org/10.1002/cne.22791

1316 Odén, A., McCloskey, E. V., Kanis, J. A., Harvey, N. C., & Johansson, H. (2015). Burden of high
1317 fracture probability worldwide: secular increases 2010–2040. *Osteoporosis*
1318 *International*, *26*(9), 2243–2248. https://doi.org/10.1007/s00198-015-3154-6

1319 Ofer, L., Dean, M. N., Zaslansky, P., Kult, S., Shwartz, Y., Zaretsky, J., Griess-Fishheimer, S.,
1320 Monsonego-Ornan, E., Zelzer, E., & Shahar, R. (2019). A novel nonosteocytic regulatory
1321 mechanism of bone modeling. *PLOS Biology*, *17*(2), e3000140.
1322 https://doi.org/10.1371/journal.pbio.3000140

1323 Ohgo, S., Ichinose, S., Yokota, H., Sato-Maeda, M., Shoji, W., & Wada, N. (2019). Tissue
1324 regeneration during lower jaw restoration in zebrafish shows some features of
1325 epimorphic regeneration. *Development, Growth & Differentiation*, dgd.12625.
1326 https://doi.org/10.1111/dgd.12625

1327 Ohnmacht, J., Yang, Y., Maurer, G. W., Barreiro-Iglesias, A., Tsarouchas, T. M., Wehner, D.,
1328 Sieger, D., Becker, C. G., & Becker, T. (2016). Spinal motor neurons are regenerated
1329 after mechanical lesion and genetic ablation in larval zebrafish. *Development*
1330 *(Cambridge)*, *143*(9), 1464–1474. https://doi.org/10.1242/dev.129155

1331 Ohno, M., Nikaido, M., Horiuchi, N., Kawakami, K., & Hatta, K. (2021). The enteric nervous
1332 system in zebrafish larvae can regenerate via migration into the ablated area and
1333 proliferation of neural crest-derived cells. *Development*, *148*(2), dev195339.
1334 https://doi.org/10.1242/dev.195339

1335 Paredes, A. D., Benavidez, D., Cheng, J., Mangos, S., Patil, R., Donoghue, M., Benedetti, E., &
1336 Bartholomew, A. (2019). The Effect of Fluence on Macrophage Kinetics, Oxidative
1337 Stress, and Wound Closure Using Real-Time In Vivo Imaging. *Photobiomodulation,*
1338 *Photomedicine, and Laser Surgery*, *37*(1), 45–52.
1339 https://doi.org/10.1089/photob.2018.4494

1340 Parichy, D. M., Elizondo, M. R., Mills, M. G., Gordon, T. N., & Engeszer, R. E. (2009). Normal

table of postembryonic zebrafish development: Staging by externally visible anatomy of the living fish. *Developmental Dynamics*, *238*(12), 2975–3015. https://doi.org/10.1002/dvdy.22113

Paul, S., Schindler, S., Giovannone, D., de Millo Terrazzani, A., Mariani, F. V, & Crump, J. G. (2016). Ihha induces hybrid cartilage-bone cells during zebrafish jawbone regeneration. *Development (Cambridge, England)*, *143*(12), 2066–2076. https://doi.org/10.1242/dev.131292

Peri, F., & Nüsslein-Volhard, C. (2008). Live Imaging of Neuronal Degradation by Microglia Reveals a Role for v0-ATPase a1 in Phagosomal Fusion In Vivo. *Cell*, *133*(5), 916–927. https://doi.org/10.1016/j.cell.2008.04.037

Peti-Peterdi, J., Kidokoro, K., & Riquier-Brison, A. (2016). Intravital imaging in the kidney. In *Current Opinion in Nephrology and Hypertension* (Vol. 25, Issue 3, pp. 168–173). Lippincott Williams and Wilkins. https://doi.org/10.1097/MNH.0000000000000219

Petrie, T. A., Strand, N. S., Yang, C.-T., Tsung-Yang, C., Rabinowitz, J. S., & Moon, R. T. (2014). Macrophages modulate adult zebrafish tail fin regeneration. *Development (Cambridge, England)*, *141*(13), 2581–2591. https://doi.org/10.1242/dev.098459

Pettit, A. R., Chang, M. K., Hume, D. A., & Raggatt, L.-J. (2008). Osteal macrophages: A new twist on coupling during bone dynamics. *Bone*, *43*(6), 976–982. https://doi.org/10.1016/j.bone.2008.08.128

Phan, Q. T., Liu, R., Tan, W. H., Imangali, N., Cheong, B., Schartl, M., & Winkler, C. (2020). Macrophages Switch to an Osteo-Modulatory Profile Upon RANKL Induction in a Medaka (Oryzias latipes) Osteoporosis Model. *JBMR Plus*, *4*(11). https://doi.org/10.1002/jbm4.10409

Phan, Q. T., Tan, W. H., Liu, R., Sundaram, S., Buettner, A., Kneitz, S., Cheong, B., Vyas, H., Mathavan, S., Schartl, M., & Winkler, C. (2020). Cxcl9l and Cxcr3.2 regulate recruitment of osteoclast progenitors to bone matrix in a medaka osteoporosis model. *Proceedings of the National Academy of Sciences of the United States of America*, *117*(32), 19276–19286. https://doi.org/10.1073/pnas.2006093117

Purwar, R., Kraus, M., Werfel, T., & Wittmann, M. (2008). Modulation of keratinocyte-

derived MMP-9 by IL-13: A possible role for the pathogenesis of epidermal inflammation. *Journal of Investigative Dermatology*, *128*(1), 59–66. https://doi.org/10.1038/sj.jid.5700940

Quinn, J. M. W., Neale, S., Fujikawa, Y., McGee, J. D., & Athanasou, N. A. (1998). Human osteoclast formation from blood monocytes, peritoneal macrophages, and bone marrow cells. *Calcified Tissue International*, *62*(6), 527–531. https://doi.org/10.1007/s002239900473

Redd, M. J., Kelly, G., Dunn, G., Way, M., & Martin, P. (2006). Imaging macrophage chemotaxis in vivo: Studies of microtubule function in zebrafish wound inflammation. *Cell Motility and the Cytoskeleton*, *63*(7), 415–422. https://doi.org/10.1002/cm.20133

Renshaw, S. A., Loynes, C. A., Trushell, D. M. I., Elworthy, S., Ingham, P. W., & Whyte, M. K. B. (2006). A transgenic zebrafish model of neutrophilic inflammation. *Blood*, *108*(13), 3976–3978. https://doi.org/10.1182/blood-2006-05-024075

Renshaw, S. A., & Trede, N. S. (2012). A model 450 million years in the making: zebrafish and vertebrate immunity. *Disease Models & Mechanisms*, *5*(1), 38–47. https://doi.org/10.1242/dmm.007138

Rhen, T., & Cidlowski, J. A. (2005). Antiinflammatory Action of Glucocorticoids — New Mechanisms for Old Drugs. *New England Journal of Medicine*, *353*(16), 1711–1723. https://doi.org/10.1056/NEJMra050541

Robertson, A. L., Ogryzko, N. V, Henry, K. M., Loynes, C. A., Foulkes, M. J., Meloni, M. M., Wang, X., Ford, C., Jackson, M., Ingham, P. W., Wilson, H. L., Farrow, S. N., Solari, R., Flower, R. J., Jones, S., Whyte, M. K. B., & Renshaw, S. A. (2016). Identification of benzopyrone as a common structural feature in compounds with anti-inflammatory activity in a zebrafish phenotypic screen. *Disease Models & Mechanisms*, *9*(6), 621–632. https://doi.org/10.1242/dmm.024935

Robinson, J. M. (2008). Reactive oxygen species in phagocytic leukocytes. In *Histochemistry and Cell Biology* (Vol. 130, Issue 2, pp. 281–297). Springer. https://doi.org/10.1007/s00418-008-0461-4

Romero, M. M. G., McCathie, G., Jankun, P., & Roehl, H. H. (2018). Damage-induced reactive

oxygen species enable zebrafish tail regeneration by repositioning of Hedgehog expressing cells. *Nature Communications*, *9*(1), 1–11. https://doi.org/10.1038/s41467-018-06460-2

Rosowski, E. E. (2020). Determining macrophage versus neutrophil contributions to innate immunity using larval zebrafish. In *Disease models & mechanisms* (Vol. 13, Issue 1). NLM (Medline). https://doi.org/10.1242/dmm.041889

Roy, S., Khanna, S., Nallu, K., Hunt, T. K., & Sen, C. K. (2006). Dermal wound healing is subject to redox control. *Molecular Therapy*, *13*(1), 211–220. https://doi.org/10.1016/j.ymthe.2005.07.684

Ru, J. ying, & Wang, Y. fen. (2020). Osteocyte apoptosis: the roles and key molecular mechanisms in resorption-related bone diseases. In *Cell Death and Disease* (Vol. 11, Issue 10, pp. 1–24). Springer Nature. https://doi.org/10.1038/s41419-020-03059-8

Russo-Marie, F. (1992). Macrophages and the glucocorticoids. *Journal of Neuroimmunology*, *40*(2–3), 281–286. http://www.ncbi.nlm.nih.gov/pubmed/1430158

Sanderson, L. E., Chien, A.-T., Astin, J. W., Crosier, K. E., Crosier, P. S., & Hall, C. J. (2015). An inducible transgene reports activation of macrophages in live zebrafish larvae. *Developmental and Comparative Immunology*, *53*(1), 63–69. https://doi.org/10.1016/j.dci.2015.06.013

Serbedzija, G. N., Chen, J., & Fishman, M. C. (1998). Regulation in the heart field of zebrafish. *Development*, *125*, 1095–1101.

Serowoky, M. A., Arata, C. E., Crump, J. G., & Mariani, F. V. (2020). Skeletal stem cells: Insights into maintaining and regenerating the skeleton. In *Development (Cambridge)* (Vol. 147, Issue 5). Company of Biologists Ltd. https://doi.org/10.1242/dev.179325

Sharif, F., de Bakker, M. A. G., & Richardson, M. K. (2014). Osteoclast-like Cells in Early Zebrafish Embryos. *Cell Journal*, *16*(2), 211–224. http://www.ncbi.nlm.nih.gov/pubmed/24567948

Sharif, F., Steenbergen, P. J., Metz, J. R., & Champagne, D. L. (2015). Long-lasting effects of dexamethasone on immune cells and wound healing in the zebrafish. *Wound Repair*

and Regeneration, *23*(6), 855–865. https://doi.org/10.1111/wrr.12366

Shiflett, L. A., Tiede-Lewis, L. A. M., Xie, Y., Lu, Y., Ray, E. C., & Dallas, S. L. (2019). Collagen Dynamics During the Process of Osteocyte Embedding and Mineralization. *Frontiers in Cell and Developmental Biology*, *7*. https://doi.org/10.3389/fcell.2019.00178

Shwartz, A., Goessling, W., & Yin, C. (2019). Macrophages in Zebrafish Models of Liver Diseases. In *Frontiers in immunology* (Vol. 10, p. 2840). NLM (Medline). https://doi.org/10.3389/fimmu.2019.02840

Sieger, D., Moritz, C., Ziegenhals, T., Prykhozhij, S., & Peri, F. (2012). Long-Range Ca2+ Waves Transmit Brain-Damage Signals to Microglia. *Developmental Cell*, *22*(6), 1138–1148. https://doi.org/10.1016/j.devcel.2012.04.012

Sinder, B. P., Pettit, A. R., & McCauley, L. K. (2015). Macrophages: Their Emerging Roles in Bone. *Journal of Bone and Mineral Research : The Official Journal of the American Society for Bone and Mineral Research*, *30*(12), 2140–2149. https://doi.org/10.1002/jbmr.2735

Singh, S. P., Holdway, J. E., & Poss, K. D. (2012). Regeneration of amputated zebrafish fin rays from de novo osteoblasts. *Developmental Cell*, *22*(4), 879–886. https://doi.org/10.1016/j.devcel.2012.03.006

Singleman, C., & Holtzman, N. G. (2014). Growth and maturation in the zebrafish, Danio Rerio: A staging tool for teaching and research. *Zebrafish*, *11*(4), 396–406. https://doi.org/10.1089/zeb.2014.0976

Smutny, M., Behrndt, M., Campinho, P., Ruprecht, V., & Heisenberg, C. P. (2015). UV laser ablation to measure cell and tissue-generated forces in the zebrafish embryo in vivo and ex vivo. *Methods in Molecular Biology*, *1189*, 219–235. https://doi.org/10.1007/978-1-4939-1164-6_15

Sousa, S., Afonso, N., Bensimon-Brito, A., Fonseca, M., Simões, M., Leon, J., Roehl, H., Cancela, M. L., Jacinto, A., Amsterdam, A., Chung, B.-C., Westerfield, M., Haffter, P., Hopkins, N., Kimmel, C., Postlethwait, J. H., & Nissen, R. (2011). Differentiated skeletal cells contribute to blastema formation during zebrafish fin regeneration. *Development (Cambridge, England)*, *138*(18), 3897–3905. https://doi.org/10.1242/dev.064717

1456 Sousa, S., Valerio, F., & Jacinto, A. (2012). A new zebrafish bone crush injury model. *Biology*
1457 *Open*, *1*(9), 915–921. https://doi.org/10.1242/bio.2012877

1458 Spoorendonk, K. M., Peterson-Maduro, J., Renn, J., Trowe, T., Kranenbarg, S., Winkler, C., &
1459 Schulte-Merker, S. (2008). Retinoic acid and Cyp26b1 are critical regulators of
1460 osteogenesis in the axial skeleton. *Development*, *135*(22), 3765–3774.
1461 https://doi.org/10.1242/dev.024034

1462 Stout, R. D., Jiang, C., Matta, B., Tietzel, I., Watkins, S. K., & Suttles, J. (2005). Macrophages
1463 sequentially change their functional phenotype in response to changes in
1464 microenvironmental influences. *Journal of Immunology (Baltimore, Md. : 1950)*, *175*(1),
1465 342–349. https://doi.org/10.4049/JIMMUNOL.175.1.342

1466 Suarez-Bregua, P., Saxena, A., Bronner, M. E., & Rotllant, J. (2017). Targeted Pth4-expressing
1467 cell ablation impairs skeletal mineralization in zebrafish. *PLoS ONE*, *12*(10).
1468 https://doi.org/10.1371/journal.pone.0186444

1469 Takayanagi, H. (2007). Osteoimmunology: shared mechanisms and crosstalk between the
1470 immune and bone systems. *Nature Reviews Immunology*, *7*(4), 292–304.
1471 https://doi.org/10.1038/nri2062

1472 Tan, H. Y., Wang, N., Li, S., Hong, M., Wang, X., & Feng, Y. (2016). The Reactive Oxygen
1473 Species in Macrophage Polarization: Reflecting Its Dual Role in Progression and
1474 Treatment of Human Diseases. In *Oxidative Medicine and Cellular Longevity* (Vol. 2016).
1475 https://doi.org/10.1155/2016/2795090

1476 Tarasco, M., Laizé, V., Cardeira, J., Cancela, M. L., & Gavaia, P. J. (2017). The zebrafish
1477 operculum: A powerful system to assess osteogenic bioactivities of molecules with
1478 pharmacological and toxicological relevance. *Comparative Biochemistry and*
1479 *Physiology. Toxicology & Pharmacology : CBP*, *197*, 45–52.
1480 https://doi.org/10.1016/j.cbpc.2017.04.006

1481 Teh, C., Chudakov, D. M., Poon, K. L., Mamedov, I. Z., Sek, J. Y., Shidlovsky, K., Lukyanov, S.,
1482 & Korzh, V. (2010). Optogenetic in vivo cell manipulation in KillerRed-expressing
1483 zebrafish transgenics. *BMC Developmental Biology*, *10*(1), 110.
1484 https://doi.org/10.1186/1471-213X-10-110

1485 To, T. T., Witten, P. E., Huysseune, A., & Winkler, C. (2015). An adult osteopetrosis model in
1486 medaka reveals the importance of osteoclast function for bone remodeling in teleost
1487 fish. *Comparative Biochemistry and Physiology. Toxicology & Pharmacology : CBP*, *178*,
1488 68–75. https://doi.org/10.1016/j.cbpc.2015.08.007

1489 Tokarz, D., Cisek, R., Wein, M. N., Turcotte, R., Haase, C., Yeh, S.-C. A., Bharadwaj, S.,
1490 Raphael, A. P., Paudel, H., Alt, C., Liu, T.-M., Kronenberg, H. M., & Lin, C. P. (2017).
1491 Intravital imaging of osteocytes in mouse calvaria using third harmonic generation
1492 microscopy. *PLOS ONE*, *12*(10), e0186846.
1493 https://doi.org/10.1371/journal.pone.0186846

1494 Tonelli, F., Cotti, S., Leoni, L., Besio, R., Gioia, R., Marchese, L., Giorgetti, S., Villani, S.,
1495 Gistelinck, C., Wagener, R., Kobbe, B., Fiedler, I. A. K., Larionova, D., Busse, B., Eyre, D.,
1496 Rossi, A., Witten, P. E., & Forlino, A. (2020). Crtap and p3h1 knock out zebrafish support
1497 defective collagen chaperoning as the cause of their osteogenesis imperfecta
1498 phenotype. *Matrix Biology*, *90*, 40–60. https://doi.org/10.1016/j.matbio.2020.03.004

1499 Trede, N. S., Langenau, D. M., Traver, D., Look, A. T., & Zon, L. I. (2004). The use of zebrafish
1500 to understand immunity. *Immunity*, *20*(4), 367–379.
1501 http://www.ncbi.nlm.nih.gov/pubmed/15084267

1502 Walton, E. M., Cronan, M. R., Beerman, R. W., & Tobin, D. M. (2015). The Macrophage-
1503 Specific Promoter mfap4 Allows Live, Long-Term Analysis of Macrophage Behavior
1504 during Mycobacterial Infection in Zebrafish. *PLOS ONE*, *10*(10), e0138949.
1505 https://doi.org/10.1371/journal.pone.0138949

1506 Wang, X., He, H., Tang, W., Zhang, X. A., & Hua, X. (2012). Two Origins of Blastemal
1507 Progenitors Define Blastemal Regeneration of Zebrafish Lower Jaw. *PLoS ONE*, *7*(9),
1508 45380. https://doi.org/10.1371/journal.pone.0045380

1509 Wauquier, F., Leotoing, L., Coxam, V., Guicheux, J., & Wittrant, Y. (2009). Oxidative stress in
1510 bone remodelling and disease. In *Trends in Molecular Medicine* (Vol. 15, Issue 10, pp.
1511 468–477). Elsevier Ltd. https://doi.org/10.1016/j.molmed.2009.08.004

1512 Weinstein, R. S. (2012). Glucocorticoid-induced osteoporosis and osteonecrosis.
1513 *Endocrinology and Metabolism Clinics of North America*, *41*(3), 595–611.

https://doi.org/10.1016/j.ecl.2012.04.004

Witten, P. E., & Huysseune, A. (2009). A comparative view on mechanisms and functions of skeletal remodelling in teleost fish, with special emphasis on osteoclasts and their function. *Biological Reviews*, *84*(2), 315–346. https://doi.org/10.1111/j.1469-185X.2009.00077.x

Woodfin, A., Voisin, M.-B., Beyrau, M., Colom, B., Caille, D., Diapouli, F.-M., Nash, G. B., Chavakis, T., Albelda, S. M., Rainger, G. E., Meda, P., Imhof, B. A., & Nourshargh, S. (2011). The junctional adhesion molecule JAM-C regulates polarized transendothelial migration of neutrophils in vivo. *Nature Immunology*, *12*(8), 761–769. https://doi.org/10.1038/ni.2062

Wynn, T. A., Chawla, A., & Pollard, J. W. (2013). Macrophage biology in development, homeostasis and disease. *Nature*, *496*(7446), 445–455. https://doi.org/10.1038/nature12034

Xie, Y., Tolmeijer, S., Oskam, J. M., Tonkens, T., Meijer, A. H., & Schaaf, M. J. M. (2019). Glucocorticoids inhibit macrophage differentiation towards a pro-inflammatory phenotype upon wounding without affecting their migration. *DMM Disease Models and Mechanisms*, *12*(5). https://doi.org/10.1242/dmm.037887

Yang, Y., Hippensteel, J. A., & Schmidt, E. P. (2018). Intravital microscopy in the mouse lung. In *Methods in Molecular Biology* (Vol. 1809, pp. 331–339). Humana Press Inc. https://doi.org/10.1007/978-1-4939-8570-8_21

Yoo, S. K., Freisinger, C. M., LeBert, D. C., & Huttenlocher, A. (2012). Early redox, Src family kinase, and calcium signaling integrate wound responses and tissue regeneration in zebrafish. *Journal of Cell Biology*, *199*(2), 225–234. https://doi.org/10.1083/jcb.201203154

Zhang, H., Wang, X., Lyu, K., Gao, S., Wang, G., Fan, C., Zhang, X. A., & Yan, J. (2015). Time point-based integrative analyses of deep-transcriptome identify four signal pathways in blastemal regeneration of zebrafish lower jaw. *Stem Cells*, *33*(3), 806–818. https://doi.org/10.1002/stem.1899

Zhang, J., Jeradi, S., Strähle, U., & Akimenko, M. A. (2012). Laser ablation of the sonic

hedgehog-a-expressing cells during fin regeneration affects ray branching morphogenesis. *Developmental Biology*, *365*(2), 424–433. https://doi.org/10.1016/j.ydbio.2012.03.008

Supplemental Information:

Supplemental fig.1

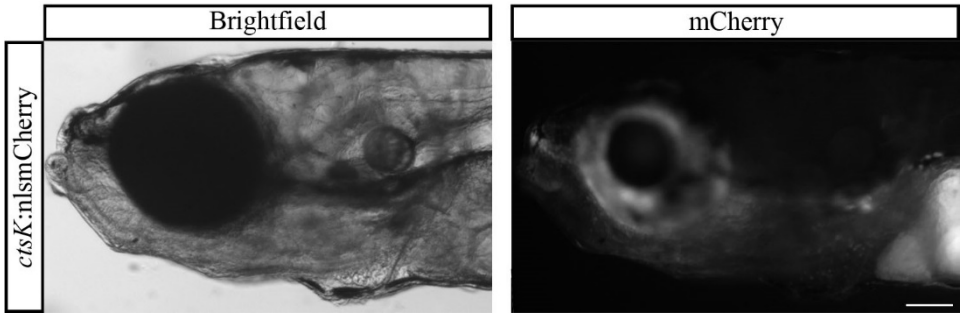

Fig. S1: Representative whole-mount image of transgenic *ctsK*:nlsmCherry larval heads at 13 dpf. The staining is visible in the whole lower jaw region. Scale bar = 100 µm. n = 2

Supplemental fig.2

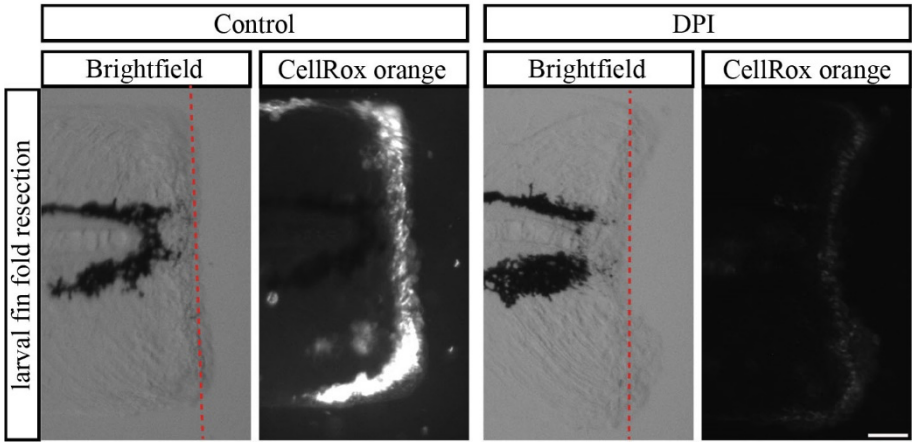

Fig. S2: Representative whole-mount images of ROS production, indicated by CellROX orange staining, 20 min after fin fold resection. The release of ROS can be blocked by a pre-treatment with the antioxidant DPI (diphenyleneiodonium). Scale bar = 50 µm. n = 6

Supplemental fig.3

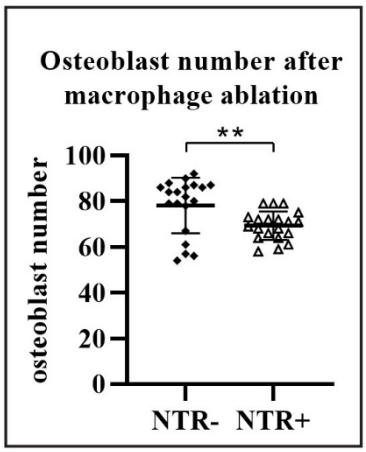

Fig. S3: Quantification of the number of osteoblasts on the uninjured opercle after ablation of macrophages with NFP. *osterix:*RFP x *mpeg1:*YFP-NTR larvae and *mpeg1*:YFP-NTR negative siblings were incubated for 6 days with NFP. A reduced number of osteoblasts at 9 dpf was detected in case of macrophages ablation. n = 20.

Movie 1 (supplement to Fig. 2): Movie showing a proliferating osteoblast in the opercle *of osterix*:nGFP transgenic zebrafish after osteoblast ablation. The position of the proliferating osteoblast is indicated by the white arrow. Division can be observed after roughly 4 h. Scale bar = 10 µm.

Movie 2 (supplement to Fig. 3C): Movie showing absence of CellRox orange staining in a transgenic 6 dpf *osterix*:nGFP zebrafish with osteoblast ablation. Scale bar = 10 µm.

Movie 3 (supplement to Fig. 3C): Movie showing increasing CellRox orange staining, as a readout for ROS release, in a transgenic 6 dpf *osterix*:nGFP zebrafish after osteoblast ablation. The increase of ROS is observed immediately lesion. Scale bar = 10 µm.

Movie 4 (supplement to Fig. 4A): Movie showing the recruitment of neutrophils, labeled in magenta, into the area of osteoblast lesion. Scale bar = 10 µm.

Movie 5 (supplement to Fig. 4C): Movie showing the recruitment of macrophages, labeled in magenta, into the area of osteoblast lesion. Scale bar = 10 µm.

Movie 6 (supplement to Fig. 4E): Movie showing the recruitment of macrophages from the surrounding tissue and not from blood vessels after osteoblast lesion. Scale bar = 20 µm.

Movie 7 (supplement to Fig. 6): Movie showing the impaired recruitment of macrophages, labeled in magenta, into the area of osteoblast lesion after pre-treatment with the antioxidant DPI. Scale bar = 10 µm.

Movie 8 (supplement to Fig. 7B): Movie showing recruitment of macrophages, labeled in magenta, into the area of osteoblast lesion after DMSO treatment. The response is comparable to the untreated response observed in laser-ablated, otherwise untreated zebrafish (see Movie 5). Scale bar = 10 µm.

Movie 9 (supplement to Fig. 7B): Movie showing reduced recruitment of macrophages, labeled in magenta, into the area of osteoblast lesion after prednisolone treatment. Please compare with the response in control treated (Movie 7) and untreated (see Movie 5) individuals. Scale bar = 10 µm.

Movie 10 (supplement to Fig. 8B): Movie showing recruitment of macrophages, labeled in magenta, into the area of a small osteoblast lesion after DMSO treatment. The response is weaker compared to the response observed in the larger laser-ablated osteoblast lesioned, otherwise untreated zebrafish (see Movie 5). Scale bar = 10 µm.

Movie 11 (supplement to Fig. 8B): Movie showing reduced recruitment of macrophages, labeled in magenta, into the area of a small osteoblast lesion after prednisolone treatment. Please compare with the response in control treated (Movie 9) and larger lesion prednisolone treated (see Movie 8) individuals. Scale bar = 10 µm.